

Cascadia Convergent Zone: An Example of Primary Convergent Seismogenic Structure

Kenneth M. Cruikshank, Curt D. Peterson

Department of Geology, Portland State University, Portland, Oregon, USA

Email: CruikshankK@pdx.edu, Curt.D.Peterson@gmail.com

How to cite this paper: Cruikshank, K.M. and Peterson, C.D. (2019) Cascadia Convergent Zone: An Example of Primary Convergent Seismogenic Structure. *Open Journal of Earthquake Research*, 8, 132-164. <https://doi.org/10.4236/ojer.2019.82009>

Received: May 3, 2019

Accepted: May 28, 2019

Published: May 31, 2019

Copyright © 2019 by author(s) and Scientific Research Publishing Inc. This work is licensed under the Creative Commons Attribution International License (CC BY 4.0).

<http://creativecommons.org/licenses/by/4.0/>



Open Access

Abstract

In this article, a case is made for very-large or primary seismogenic structures in convergent margins, based on anomalous large earthquake magnitudes (M_w 8 - 9) relative to rupture lengths. Out of 56,293 earthquakes (magnitudes ≥ 5) cataloged worldwide, the 10 largest events in transform, divergent, and interior settings average magnitudes of 7.3 - 7.6. But in convergent margins, the average magnitude of the 10 largest events is 8.5, roughly 32 times more energy than the other neotectonic settings. The large anomalous magnitudes of energy release in convergent margins are attributed to the transfer of inter-plate stress to the upper-plate, where convergent elastic strain is accumulated during interseismic intervals. The large volumes of rock that accumulate the elastic strain in the upper-plates of convergent zones are defined here as primary seismogenic structures. Several datasets of 1) modern upper-plate convergent strain, 2) historical earthquakes, 3) modern upper-plate vertical displacements, and 4) recent inter-plate events of Episodic Tremor and Slip (ETS) are compared to establish the extent of the primary seismogenic structure in the Cascadia convergent zone. The across-margin extents of 1) significant convergent strain, 2) margin-parallel bands of vertical displacement, 3) historical seismicity and 4) ETS events, representing inter-plate coupling and shear stress transfer to strain accumulation in the upper-plate, are used to map the width of the primary seismogenic structure. The across-margin width of the primary seismogenic structure in the central Cascadia margin ranges from 300 km in the south-central margin to 450 km in the north-central margin, as mapped landward from the buried trench. A broad source region of coseismic energy release in the Cascadia primary seismogenic structure (300 - 450 km width) could yield stronger shaking in interior metropolitan centers from a future major rupture of the mega-thrust than has been modeled from a narrow "locked" zone located offshore under the outer continental shelf. Despite low dip angle and associated wide inter-plate coupling, the Cascadia margin likely serves as an example of inter-plate shear

stress transfer to elastic strain accumulation in the upper-plate of some other well-coupled convergent margins worldwide.

Keywords

Subduction Zone, Crustal Structure, Seismicity, Strain, Deformation

1. Introduction

In earthquake-related neo-tectonics, faults are usually the focus of earthquake prediction/forecast studies. In this paper, we shift the focus from individual faults to *seismogenic structures* which we define as the volume of rock that releases energy in an earthquake. A seismogenic structure is an assemblage of smaller structures such as faults and folds, so its spatial scale exceeds any individual fault/fold structure. The evolution of what we would define as a seismogenic structure was recently observed in 14 November 2016, New Zealand, earthquake (M 7.8) and summarized by Mason [1] (in an editorial, referring to a paper by Hamling, Hreinsdóttir [2]):

“A reassuring rule of thumb about earthquakes is breaking down. For decades, seismologists had assumed that individual faults—as well as isolated segments of longer faults—rupture independently of one another. That limits the maximum size of the potential earthquake that a fault zone can generate. But the magnitude-7.8 earthquake that struck New Zealand just after midnight on 14 November 2016—among the largest in the islands’ modern history has reduced that thinking to rubble. According to a new study, published online this week in Science, the heavy shaking in the Kaikoura quake was amassed by ruptures on at least 12 different faults, in some cases so far apart that they were thought to be immune to each other’s influence.”

The New Zealand 2016 earthquake is not unique, as similar observations have been reported following some other earthquakes [3], including events such as the 1983 Coalinga earthquake [4] [5] [6], and in the Borrego Mountain—Superstition Hills—Imperial Valley earthquake sequence [7] [8]. Within a large seismogenic structure, multiple crustal faults are often activated during a system-wide energy release from the seismogenic structure. The seismogenic system can be more extensive than adjacent fault segments within a fault zone (e.g., [9] [10] [11]). This may explain why focal mechanisms for some crustal earthquakes, including multiple fault segments, deviate from the ideal double-couple mechanism [12] [13].

Seismogenic structures are consistent with experience from structural geology. Crustal faults are part of an ensemble of faults and folds that enable a larger structure to evolve. Crustal faults can also occur as distinct systems (sets) of different orientations [14] [15] within the larger strain field(s) of hosting seismogenic structures. Early studies of convergent margin earthquakes, recognized the

broad extent of “crustal” or upper-plate deformation [16] but with advances in plate tectonic theory, seismogenic studies focused on inter-plate displacement modeling [17] [18]. However, post-earthquake surveys at convergent plate subduction zones suggest that in addition to the “locked-zone” fault displacements, there are also portions of the upper-plate deformation that come from “unfolding” of the “crust” [16] [19]. For example, the recognition of multiple zero-extensions and the great landward extent of extension in the upper-plate, following the great 1964 Gulf of Alaska earthquake (M_w 9.2) demonstrate that a significant portion of upper-plate displacement comes from crustal extension [16] [20]. Unfortunately, in the current forward displacement modeling of subduction zones [21], the folding/shortening components in the upper-plates are usually ignored, leaving the sources of released seismic energy to assumed narrow “locked zones,” located well offshore of inland cities and lifeline infrastructures, and confined to a relatively narrow “locked” fault zone.

Plate boundary seismogenic structures can occur at different spatial scales. In this paper, we are concerned with what we term the *primary seismogenic structure*, which is the structure at the same scale, or larger than, the plate boundary that it comprises. Primary seismogenic structures occur from plate interactions at plate boundaries, but they can extend beyond the zone of inter-plate coupling. For example, recent interseismic- and coseismic-horizontal strains, as measured respectively, in the upper-plates of the Cascadia margin [22] [23] [24] [25] and the Tohoku margin, Japan (M_w ~9.0, 2011) [26], extended several hundred kilometers landward of the assumed inter-plate couplings. As noted above, such landward deformation of the “crust” or upper-plate, extending 400 - 500 km inland from the trench, was reported for the Gulf of Alaska rupture (M_w ~9.2; 1964) [16] [20]. In the 2010 Chile earthquake (M_w 8.8) earthquake, GPS data shows that there were about 4 cm centimeters of co-seismic displacement at stations located in eastern Argentina, some 800 km landward from the trench axis [27]. Due to the upper-plate deformation that extends landward of the inter-plate coupling or plate margin, we refer to the larger upper-plate area impacted by plate convergence as the convergent zone. This nomenclature does not discriminate between subduction, obduction or over-thrusting.

In this article, the Cascadia subduction zone (**Figure 1**) is used as an example of primary or very-large seismogenic structures that develop at convergent plate boundaries. In the case of subduction zones, such very-large structures can extend well landward of the initial zone of inter-plate coupling or the “locked zone” as modeled to occur within a few tens of kilometers of the trench [28]. Such primary seismogenic structures have the potential to generate great earthquake energies (M_w 8 - 9) from the released elastic strain that accumulates in the upper-plate during preceding interseismic intervals [22]. In the Cascadia margin, the accumulation of elastic strain in the upper-plate extends across all zones of inter-plate coupling, including intermittent coupling under the Coast Ranges and forearc valleys and recoupling under the magmatic arc [24]. The convergent

strain reaches landward distances of several hundred kilometers from the trench. To make a case for such a broad primary seismogenic structure in the Cascadia margin, previously published catalogs of recorded seismicity and episodic tremor and slip events (ETS) [29] are compared to recently published analyses of GPS station horizontal strains and vertical displacements [22] [24]. To place the anomalously large magnitudes of some convergent margin ruptures or great earthquakes (M_w 8 - 9) into the context of worldwide seismicity, relations between seismic energy release in convergent, divergent, transform, and interior neotectonic settings are compared. To justify the focus of this article on primary seismogenic structures in convergent plate margins we first review historic large-magnitude earthquakes that apparently incorporated multiple fault systems and/or unusually broad upper-plate deformation, as outlined below.

The central Cascadia margin (**Figure 1**) is a small remnant (~800 km length) of the largely subducted northern Farallon plate, and it is characterized by shallow dip angles (5° - 15°) of the relatively young (4 - 8 Ma) and buoyant Juan De Fuca oceanic plate segment **Figure 2**. Smaller and younger oceanic plate segments, the Explorer and Gorda plate segments, flank the central Juan De Fuca plate segment. A cross-section of the central Cascadia margin is shown in **Figure 2**. Under the continental shelf the Juan De Fuca plate dips landward at about 5° but increases to 7° - 10° under the Coast Range, and to $\sim 12^\circ$ under the forearc valley, at about 200 km landward (due east) of the buried trench [30]. Maximum convergent strain in the central Cascadia margin is generally oriented southwest-northeast [22], in the direction of plate convergence (**Figure 1**). However, the large linear structural elements in the central Cascadia margin, including the buried trench, the offshore fold, and thrust belt, the Coast Range, the forearc valleys, and the volcanic arc are all aligned nearly north-south.

How might the landward extent of upper-plate deformation in convergent subduction zones, such as the Cascadia margin (**Figure 1**), be related to coseismic energy release during mega-thrust ruptures? How far inland from the buried trench or deformation front can inter-seismic stress and accumulated strain be propagated and stored in the upper-plate? Such questions are increasingly relevant to safety hazards from under-reinforced infra-structure developed well away from the presumed "seismic sources" in offshore "locked zones" of subduction-zone margins [24]. In this article, we compile several previously reported datasets for the Cascadia convergent zone (**Figure 1**) that indicate both the scale and geometry of the Cascadia primary seismogenic structure. These parameters are consistent with previously reported margin-scale convergent-strain studies in the Cascadia margin [22] [24] [31].

We propose that the Cascadia convergent zone (**Figure 1**) encompasses a primary seismogenic structure (a volume of about 1.3×10^7 km³) that is much greater (5 to 10 times) than in the reported narrow "locked zone" as interpreted to underlie the continental slope and outer-continental shelf [28] [32] [33] [34] [35].

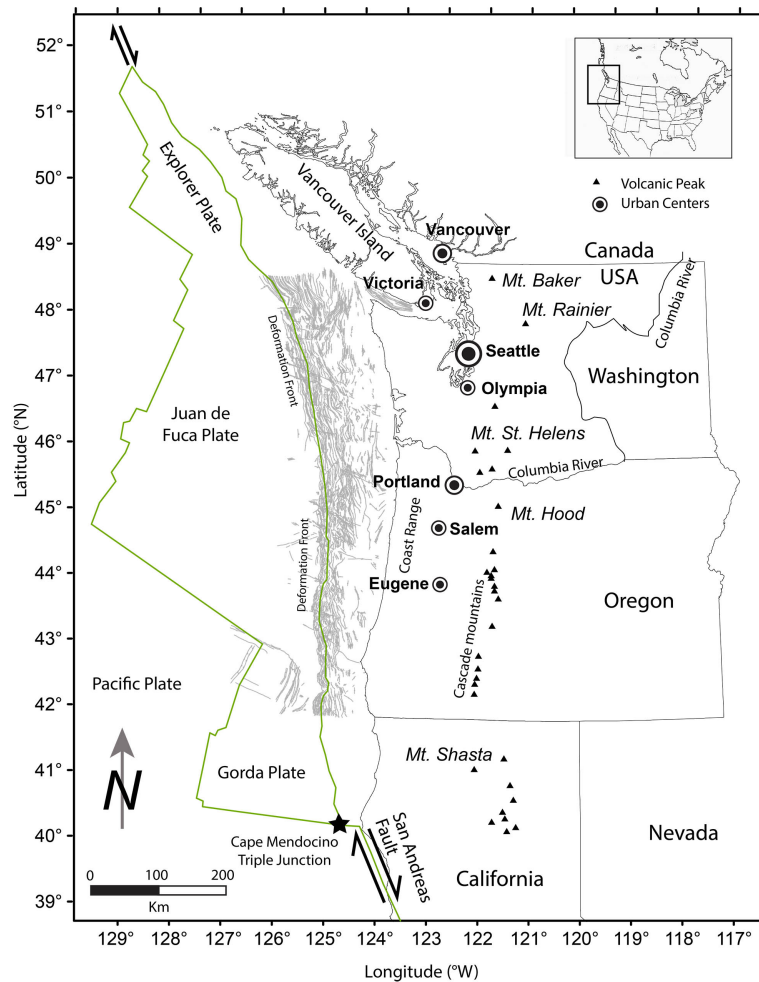


Figure 1. Location map for the Cascadia convergent margin, as composed of the Juan De Fuca plate segment (central Cascadia margin), the Explorer plate segment (northern Cascadia margin), and Gorda plate (southern Cascadia margin). We focus on the area from 41°N to 50°N and 117°W to 127.5°W.

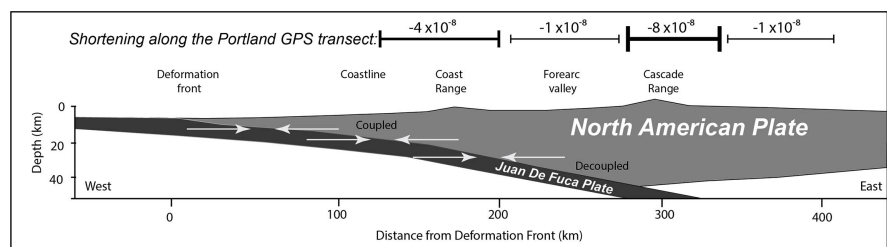


Figure 2. Illustrative cross-section (46° - 47° latitude) across the Cascadia subduction zone from the west (W) to the east (E). The Juan De Fuca (oceanic) plate descends under the North American (continental) plate at 5° (Outer-shelf) to 7° - 10° (Coast Ranges) to 12° (Cascade Range). Inter-plate coupling occurs under the continental shelf (fold and thrust belt) and uplifted Coast Ranges. Localized very-weak coupling or decoupling occurs under the Forearc Valleys (Puget Trough and Willamette). The inter-plate zone is interpreted to recouple against the base of the Cascade volcanic arc (dashed line at seismic velocity break between 7.7 km/s and 7.8 km/s). Horizontal strains decrease from the coast to the Cascade Range, where they locally increase before decreasing to the East. The diagram is redrawn from [31].

The Cascadia primary seismogenic structure model, as proposed here, has important implications for great earthquake shaking and related damage to major metropolitan centers in Vancouver, Canada, and Seattle, Olympia, Portland, Salem, and Eugene, USA, in the event of a future major mega-thrust rupture in the central Cascadia subduction zone. Such considerations are relevant to similar convergent margin settings around the world.

2. Data Sources

Demonstrating that the Cascadia margin could be viewed as a single seismogenic structure involves integrating a series of datasets. We start by discussing the various data sets and how they were integrated.

2.1. Earthquake Catalogs and Tectonic Settings

In this section, we identify the data sources that were integrated for analyses of recorded historical earthquakes in different tectonic settings, including the Cascadia convergent zone. The compilations of “seismic” events in the Cascadia convergent zone also include catalogs of recent Episodic Tremor and Slip (ETS) events. Transects for previously reported upper-plate strain data in the Cascadia convergent zone are shown and described. Comparisons between the modern strain data, the historical seismic record, recent ETS events from the Cascadia convergent zone are presented in the Results section of this article. In general, the worldwide earthquake catalog data [36] [37] [38] were imported into a relational database, and the various catalogs were joined by finding information in common between the datasets, mostly the catalog number. In some instances, the epoch, location, and magnitude were used to relate datasets. Datasets, such as the displacement data reported by Wells and Coppersmith [39] and others [40] [41] [42] [43] could then be joined to known events and Moment Tensor event information. Datasets were joined to the various catalog data by adding a USGS catalog number to the datasets. This method joined the offset data to the catalog event, which was tied to Flinn-Engdahl regions [44], and from there to tectonic boundary type. The USGS event was also joined to the Centroid Moment Tensor catalog and the Radiated energy catalogs. Earthquakes in the catalog could be characterized using the Flinn-Engdahl region [44]. Each Flinn-Engdahl region was then ascribed to the dominant tectonic setting of the region. The mapped tectonic boundaries were then grouped under simplified tectonic boundaries, as shown in **Table 1**. The completed database allowed for the integration of various seismological and geological observations. Database script was written to produce the tables and figures used in this article.

Earthquake catalogs can be difficult to use for tectonic analysis. For example, we focus on magnitude five and larger earthquakes in some analyses, since these are the most reliably detected by worldwide networks. Local networks, the qualities of which vary regionally, could put biases in the data, so we favor the magnitude five and larger events. We also focus on shallow- and intermediate depth events (0 - 60 km depth; [45], p. 30). Deeper events (>60 km) might not be

Table 1. Tectonic boundary types used in the earthquake database. Earthquakes are located within Flinn-Engdahl regions; each region was then assigned to a boundary type based on the dominant boundary within the region. This follows the approach used by others [47], except we use all 728 zones [44] rather than the 35 regions used by Kagan [47].

Complete Boundary	Simple Boundary
Divergent	Divergent
Divergent-Continental	Divergent
Divergent-Oceanic	Divergent
Convergent	Convergent
Convergent-Oceanic	Convergent
Convergent-Continental	Convergent
Convergent-Mixed	Convergent
Transform	Transform
Transform-Oceanic	Transform
Transform-Continental	Transform
Intraplate-Continental	Interior
Intraplate-Oceanic	Interior
Volcanic	Interior
Continental Shelf	Interior

clearly related to the surface tectonic setting, but they do have an application to mapping the descending slab or lower-plate. When using the Pacific Northwest Seismic Network events [46], volcanic earthquakes were excluded from the compilations used in this article, following the determination made by Pacific Northwest Seismic Network (which covers the central and southern Cascadia margin). If the earthquake is in their “volcanic” source list, we ignore that event. It is not 100% effective, but in bulk, it seems to eliminate the hotspots associated with the Cascade volcanoes. Lastly, we do not consider Richter-like magnitudes to be the best measure of earthquake energy. Where possible, we use the scalar moment from the Harvard CMT, or the IRIS radiated energy. We prefer radiated energy since it makes fewer assumptions

In this paper, we compile and integrate the following datasets:

- Convergent Margin Strain studies [22] [24] [26]
- PNSN Earthquake locations [46]
- PNSN First-Motion Studies [46]
- PNSN Tremor events [46]
- SPUD [48] and CHOY [49] catalogs of Radiated Seismic Energy

2.2. Upper-Plate Strain Transects in the Cascadia Convergent Zone

GPS baseline strains, *i.e.*, baseline shortening or lengthening, between 1200

paired adjacent GPS stations are well documented in the Cascadia margin [24]. Details on the methods of strain analyses are given elsewhere [22]. For the purposes of convergent strain analyses in this paper, we use selected margin perpendicular (west-east) GPS station transects, which are normal to the major linear structural elements or deformation bands in the Cascadia convergent zone (**Figure 1** and **Figure 2**). The density of GPS base stations and previously published baseline strain transects are shown in **Figure 3**. Baseline strain, averaged over decadal intervals, is normalized to annual rates of shortening (negative strain) or lengthening (positive strain) and plotted between GPS station endpoints.

2.3. Cascadia Earthquake and ETS Events

The University of Washington earthquake catalog [46] was used for compilations of a total of about 106,000 earthquakes ($-2.5 \leq M \leq 6.8$) in the Cascadia convergent zone. Earthquake data compilations include event dates, hypocenter locations, magnitudes, and first-motions. The maps in this article omit earthquake events identified in the UW catalog as belonging to volcanic activity associated

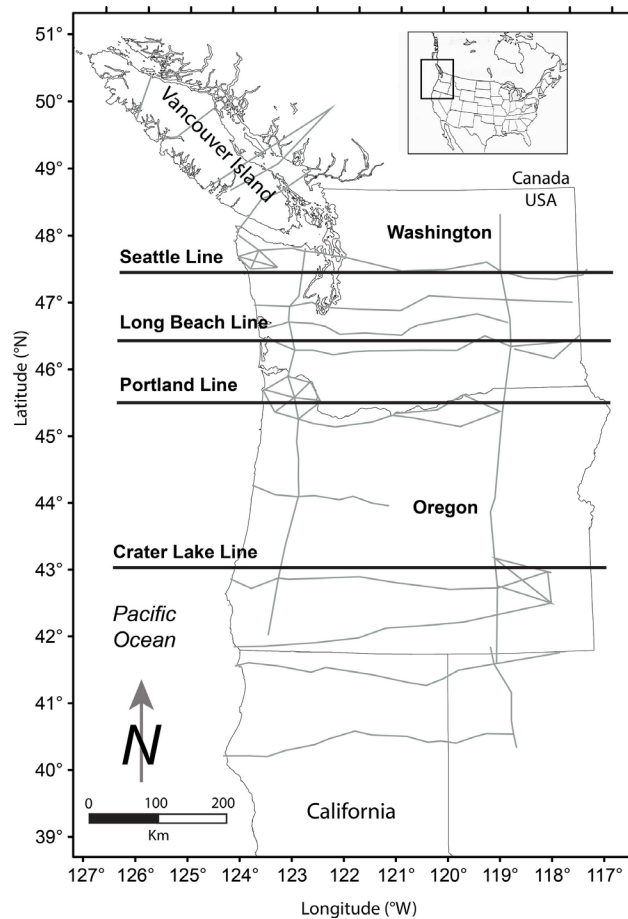


Figure 3. Plots of previously published east-west baseline strain transects (grey lines). Locations of named transects are used in this article (black lines; **Figures 9-12**). Figure modified from Cruikshank and Peterson [24].

with the various Cascade volcanoes. This does not eliminate all the probable volcanic earthquakes. Hypocenter data is shown in two ways: One is a traditional circle at the location of the earthquake; the other is as earthquake density. For earthquake density, the number of earthquakes within a small area is represented by a contour map.

For Cascadia episodic tremor and slip (ETS) events the University of Washington catalog [46] was used. Over 400,000 ETS events from the Cascadia subduction zone were compiled for this article. As with earthquake epicenters, the ETS events are contoured by density to show areas of relative concentration. The depths of ETS events are not well constrained [29] [50], but for the purposes of this article, they are assumed to lie near or within the inter-plate interface. Reported features of some ETS events include periodic displacements at annual or sub-annual time scales, including for example, an apparent westward movement of station ALBH in Victoria, British Columbia, Canada [51]. This apparent movement is relative to station DRAO in the Canadian Rockies and assumes DRAO is fixed and unmoving. The NASA/JPL data using an Earth-Centered, Earth-Fixed (ECEF) solution suggests both stations ALBH and DRAO are moving toward the southwest. DRAO (16.6 mm/yr) is moving faster than ALBH (11.3 mm/yr). The apparent relative periodic displacements between the two stations are still resolved, but they are not explained. In this article, we do not address ETS periodic movements but focus on discrete events. Details on processing and selecting ETS positions are given by Wech [29] [50].

2.4. GPS Derived Vertical Velocities

Surface GPS stations can be used to look at the variation in the vertical component of GPS station motion [24]. Though not recording vertical strain, the GPS station velocity data do demonstrate vertical deformation at the regional scale. The vertical velocity data were obtained from the Plate Boundary Observation stations, as reported by UNAVCO [52]. Preliminary test and calibrations of the regional vertical velocity data were made using previously published vertical displacement trends from 50-year geodetic releveling surveys [53].

3. Compilation of Datasets

Before examining the Cascadia margin, there are two relevant observations on the relationship between magnitude size and rupture metrics. Both suggest that at convergent margins what is happening is different from other margins. The suggestion of the existence of a primary seismogenic structure is a preferred explanation for these observations.

3.1. General Observations

3.1.1. The Case against Simple Rupture Length to Earthquake Magnitude Relations in Different Plate Margins

In this section, we use earthquake magnitude as a proxy for earthquake energy release in different types of plate margins. If all plate margins had similar seis-

mogenic structures limited to deformation at or near a fault/plate-boundary rupture, then it would be expected that all margins would have similar magnitude distributions relative to rupture lengths/areas. Under such a scenario, where the earthquake magnitude or stored energy release is proportional to fault slip length/area it would be expected that similar slip-magnitude relations would occur for all earthquakes at different tectonic margins. That is not the case. It is not as simple as longer rupture lengths correspond to larger magnitude earthquakes. Convergent margins have orders of magnitude more energy stored, and released, in their largest events [47] than do divergent or transform margins. The magnitude to slip relations for convergent margins are much greater than those for other plate margin types (Figure 4).

Plots of earthquake magnitudes (Figure 4) also show that the larger convergent margin earthquakes are separated by a “jump” in released energy compared to crustal faults and other plate margin ruptures. This suggests that there is an additional source of energy beyond what would be expected from simple faulting. These data also indicate that beyond 100 km rupture length there is not a substantial increase in seismic Moment (M_0). There have been numerous attempts to formulate relationships between magnitude and fault slip [39] [40] [41] [42] [43] [54] [55]. Most of these relationships use data that were analyzed with log-log relationships, which present difficulties when functional relationships are interpreted [56] [57]. In the case of the “jump” in earthquake magnitudes relative to rupture lengths (slip) in convergent margins, as shown in Figure 4, some additional form(s) of earthquake energy storage and release must operate beyond the fault/plate-boundary interface, as are addressed in later sections of this article.

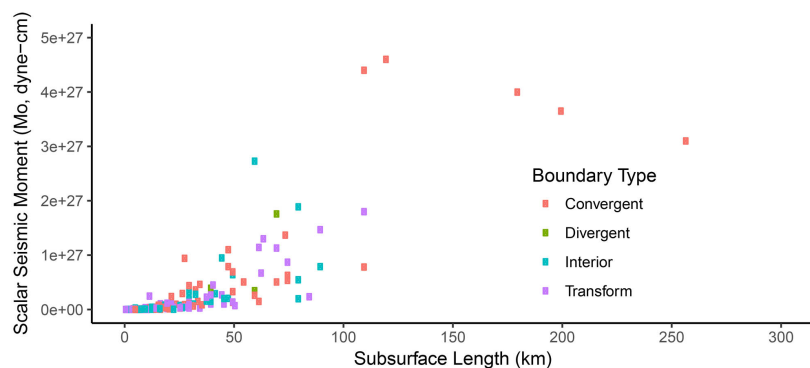


Figure 4. Fault Subsurface Length and observed scalar seismic moment for events presented in Wells and Coppersmith [39] [41] [43]. The relationship appears to change for lengths greater than about 100 km, suggesting a corresponding change in the mechanism for storing and releasing energy. Events with the largest subsurface length are all at convergent margins (red dots). Red dots represent earthquakes at convergent margins, green from divergent margins, blue from plate interiors, and purple from transform. Data from the 1957 Gobi-Altai earthquake is omitted, it had a rupture length of 240 km, but a M_0 of 1.8×10^{28} , and appears to be an outlier. M_0 was not instrumentally measured. The Wells and Coppersmith [39] values for M_0 are replaced with values from the CMT [38] project, where available.

3.1.2. Earthquake Magnitudes at Different Margin Types

A compilation of 56,293 world-wide earthquakes (magnitudes ≥ 5) from published catalogs (**Table 1**), shows differences between maximum earthquake magnitudes and tectonic margin types; convergent, divergent, transform, and plate interior.

Table 2 shows that the average magnitude for the ten largest earthquakes in transform, divergent, and interior tectonic settings range in magnitude from 7.3 to 7.6, but at convergent margins, the average is about 8.5, which represents approximately 32 times more energy than the other margins [58]. Although the average magnitude for all margins is about 5.4, there are about 5 - 17 times more earthquakes at the convergent margins, so there is proportionally, much more energy released in the convergent margin settings. These data illustrate how convergent margins (*e.g.*, Cascadia margin) are different from other types of plate margins. These differences indicate that the sizes of the corresponding seismogenic structures in convergent margins are different from other plate boundary types. This is because the principal compression is perpendicular to the margin, allowing for very large volumes of rock to accumulate inter-seismic strain energy, as delivered by convergent stresses at the inter-plate boundaries.

Convergent boundaries also contain the highest average magnitude when considering the largest ten earthquakes in each boundary. It is difficult to separate Divergent and Transform in some areas since a single FE zone may cover a ridge complex, which is made up of both transform and divergent structures. The total number of earthquakes analyzed here (56,293) are taken from published world-wide earthquake catalogs. See *Methods* section for data sources.

In summary, convergent margins produce more great earthquakes ($M_w \geq 8.0$) than any other tectonic margin (**Table 2**). The great earthquakes at convergent margins suggest that the released strain energy is probably associated with primary seismogenic structures that are much larger in volume than those from slip deficit across a narrow inter-plate or fault interface. The insights gained from studies of transform margins (*e.g.*, the San Andreas Fault; **Figure 1**) and associated crustal earthquakes (*e.g.*, 1992 Landers, 1994 Northridge, etc.) may not be transferable to understanding the very-large magnitude convergent margin earthquakes. However, such transform analog fault-slip events probably are transferable to smaller crustal fault earthquakes that occur within the upper-plate of a convergent margin, independent from major mega-thrust or great earthquake ruptures.

The compilation of 56,293 cataloged earthquakes is also sorted to identify the number of earthquakes corresponding to different magnitudes for each of the four tectonic settings: convergent, divergent, transform, and plate interior (**Table 3**). The convergent margins have the greatest number of earthquakes in the large magnitude range ($M 6 - 7$) range, and 19 of the 21 earthquakes in the great earthquake range ($M \geq 8.0$). The results as portrayed slightly differently in **Table 2** and **Table 3** highlight our concern for the vulnerable inland metropolitan centers in the Cascadia margin (**Figure 1**). This concern is based on the infrequent,

Table 2. The table shows an average magnitude of all earthquakes and average magnitude of the 10 largest earthquakes by the tectonic boundary for shallow and intermediate-depth earthquakes (depths less than 60 km). The largest earthquakes are found at convergent boundaries.

Boundary	Number of Earthquakes	Maximum Magnitude	Average Magnitude	Standard Deviation	Average of 10 Largest
Convergent	41779	9.1	5.4	0.43	8.56
Divergent	8295	8.1	5.4	0.37	7.32
Interior	3764	7.9	5.4	0.41	7.51
Transform	2455	8.2	5.4	0.45	7.65

Table 3. The frequency of events by margin type for shallow and intermediate earthquakes. Convergent margins have the largest earthquakes and a corresponding number of small earthquakes. This suggests the energy-containing structure (the seismogenic structure) is considerably larger in convergent margins than in the other types of margins. See Methods for description of earthquake data sources and relation of margin types.

	<i>Magnitude</i>								
	5	5.5	6	6.5	7	7.5	8	8.5	9
<i>Convergent</i>	31,945	6847	2107	716	203	100	14	3	2
<i>Divergent</i>	6353	1507	376	90	13	2	1	0	0
<i>Interior</i>	2919	587	198	61	18	5	0	0	0
<i>Transform</i>	1800	456	135	52	17	7	1	0	0

but very-large magnitude, great earthquakes that are associated with major ruptures of the central Cascadia margin [24] [59].

The data presented above suggest that the nature of the seismogenic structure varies by margin type. Since convergent margins have the possibility of involving the largest volume of rock as a strain accumulator, they have the largest magnitude events.

3.2. Compilation of Observations at the Cascadia Margin

In the preceding sections, we have shown that convergent margins are seismologically different from other margins. In the remainder of this article we compile reported modern strain and recent seismicity data for the Cascadia margin region. These dataset compilations and analyses are used to show how the primary seismogenic structure in the Cascadia convergent zone is expressed and how it could control great earthquake energy or magnitude during major mega-thrust ruptures. The Cascadia margin differs from some other subduction zones on the basis of 1) locally oblique plate convergence and 2) low angles of oceanic plate dip (5° - 12°) as shown respectively in **Figure 1** and **Figure 2**. However, the central portion of the Cascadia margin (**Figure 1**) is relatively uncomplicated (straight). It has a well-dated paleo-record of coseismic coastal subsidence and corresponding nearfield tsunami excitation from major mega-thrust ruptures [60] [61]. Of particular importance to the analyses presented here, the

Cascadia margin is well-instrumented for GPS station baselines [22] [24] and broadband seismograph stations [46]. However, the Cascadia margin has not experienced a great earthquake in historical time (pre-European contact), thus motivating studies of predicting potential seismic energy distributions from a future major mega-thrust rupture.

3.3. GPS Derived Strains in the Cascadia Convergent Zone

Measured convergent strains measured in GPS baselines in the Cascadia margin range from 10^{-7} a^{-1} to 10^{-9} a^{-1} [24]. Representative east-west or margin parallel strain transects are shown in **Figure 5**. Modern crustal shortening dominates across the Coast Ranges in Vancouver Island, British Columbia, the Olympic Range in northwest Washington, the Northern Coast Range in southwest Washington and Oregon, and the Siskiyou/Klamath Coast Ranges in southwest Oregon and northwest California. Convergent annual strain rates in the Coast Ranges (generally -10^{-8} a^{-1} to -10^{-7} a^{-1}) represent modern crustal shortening due to underlying inter-plate coupling and resulting shear stress transfer through the upper-plate to manifest as strain at the upper-plate surface. As will be addressed below, infrequent ETS events at or near the inter-plate interface suggest episodic slip between the plates under the Coast Ranges. Furthermore, changing strain rates in some transects [24] suggest transient strain propagation across the coupled zone, possibly related to components of aseismic slip across the coupled zone.

A landward band of little to no convergent strain (**Figure 5**) approximately coincides with the large forearc valleys (Puget Trough and Willamette River Valley) which lie between the Coast Ranges and the Cascade Range in the central Cascadia margin (**Figure 1** and **Figure 2**). This narrow band (20 - 50 km in width) is interpreted to represent a very-weakly or intermittently decoupled interface between the underlying Jan de Fuca plate and the overriding North American plate [22] [31]. As will be shown below, the maximum density of ETS events are localized in this narrow band of little to no modern convergent strain. A more landward band of anomalous high convergent strain (annual strain rates -10^{-8} a^{-1} to -10^{-7} a^{-1}) is locally present along the western side of the Cascade volcanic arc in Washington and northern Oregon and in at least one transect in southern Oregon (**Figure 5**). Crustal shortening in this narrow band suggests inter-plate coupling under the volcanic arc where the North American plate is slightly thickened [30]. Where the continental plate thins, landward (east) of the present volcanic arc the east-west GPS baselines are generally characterized by no measurable change in strain ($<10^{-9} \text{ a}^{-1}$) or by local extension. These baselines have been interpreted to represent decoupling between the upper- and lower-plates, though one transect (Long Beach transect; **Figure 10**) in central Washington demonstrated significant crustal shortening on the east side of the Cascade Range. As will be addressed below, this anomalous zone of convergent strain on the east side of the Cascade Range in Washington coincides with locally historical seismicity in the upper plate.

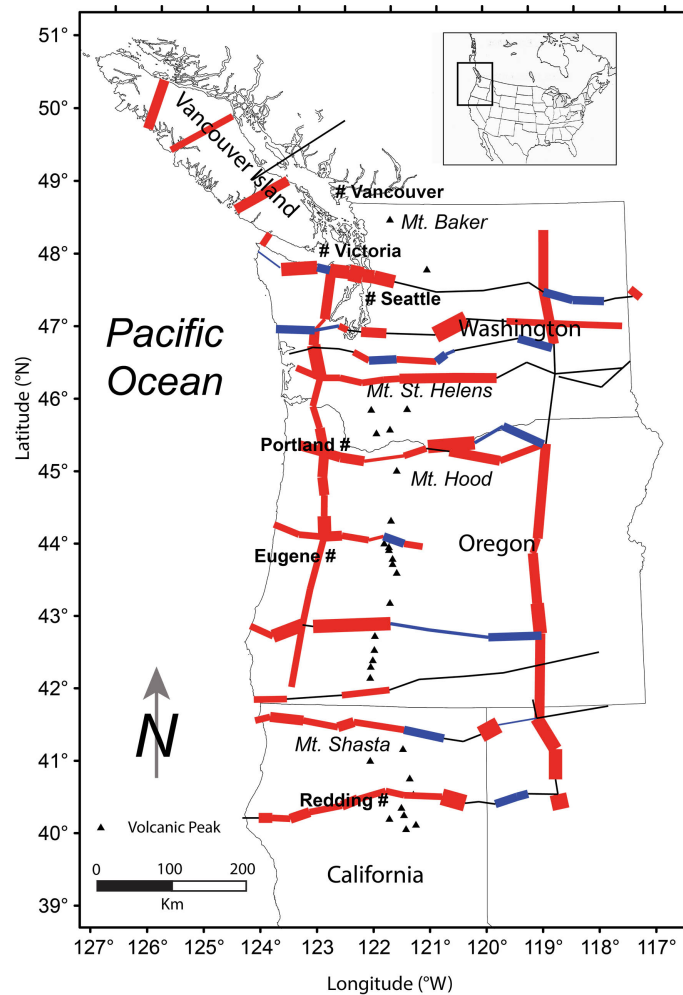


Figure 5. Selected east-west transect strain plots from Cruikshank and Peterson [24]. Lines showing the magnitude of strain (the larger the strain, the wider the line): shortening (red) no change (black) and extension (blue).

3.4. Earthquake Data for the Cascadia Convergent Zone

Plots of hypocenter location and magnitude for deeper earthquakes (>30 km depth) in the Pacific Northwest region, including the Cascadia convergent zone, and shallow earthquakes (<30 km depth) in the upper-plate are presented in **Figure 6**. The cataloged earthquakes (106,000 in number) recorded between March 1969 and May 2019 demonstrate small-magnitude ($M \leq 6.8$) releases of elastic strain energy in either the inter-plate interface or the descending slab (deeper events in **Figure 6(a)**), or the upper-crust (shallow events in **Figure 6(b)**) and offshore in the Gorda plate (**Figure 1**). The deeper inter-plate or descending slab events are concentrated in northwest Washington, where the Cascadia margin substantially bends, possibly introducing confining forces on the descending slab. Relatively little deep (inter-plate) seismicity is associated with the remainder of the central Cascadia margin (southwest Washington and Oregon), which host the most complete records of major mega-thrust rupture data, including: wide-spread coseismic coastal subsidence [59] [61] [62], nearfield

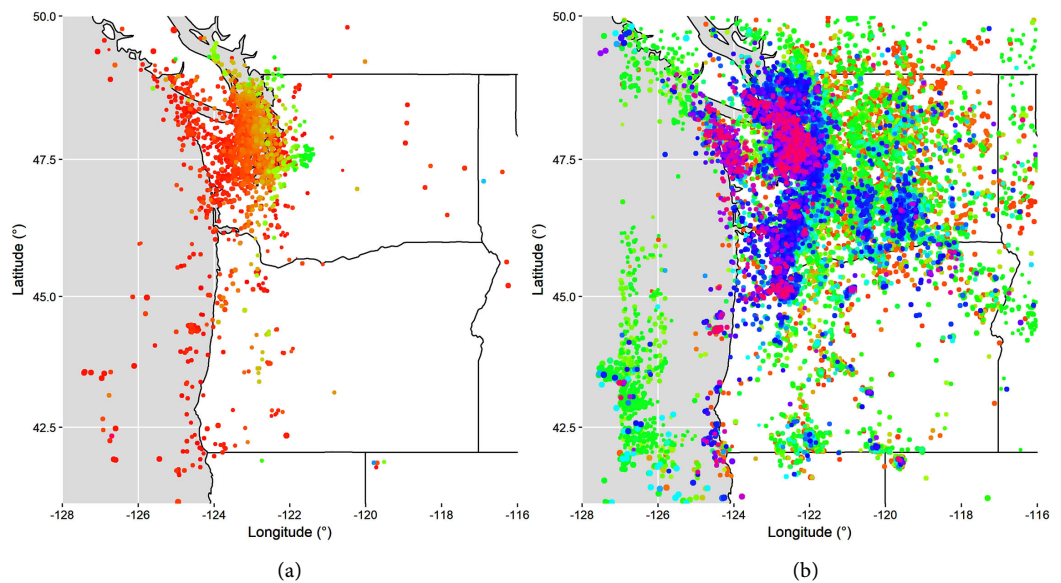


Figure 6. Distribution of earthquake epicenters in the Pacific Northwest, including Part A, deeper earthquakes (>30 km depth) and Part B, shallow earthquakes (<30 km depth). Earthquake depth and magnitude, respectively, are coded by color and dot size. Earthquakes that were reportedly associated with volcanic activity, *i.e.*, Mt. St Helens, Mt. Hood, Mt. Rainier, etc., are excluded from the plot. Many of the offshore events south of 47.5°N are related to a divergent margin.

tsunami inundation [63], and coseismic paleoliquefaction [25] [64]. The historic inter-plate seismic record does not serve as an indicator of past major mega-thrust ruptures in the Cascadia convergent zone, but it does help define the extent of the primary seismogenic structure.

The distributions of cataloged smaller-magnitude earthquakes ($M \leq 6.8$) compare well to modern convergent strain in the upper- and lower-plates (**Figure 5** and **Figure 6(b)**). Relatively dense distributions of shallow earthquake events (≤ 30 km depth) indicate stress/strain resulting from convergence of the Juan de Fuca and North American plates and extending to about 400 - 500 km from the buried trench (also referred to as the Cascadia deformation front) in Washington and northern Oregon. The frequency and magnitude of historical seismicity decrease dramatically in southern Oregon, where infrequent upper-plate seismic events reach distances of 300 km from the buried trench. As will be shown below, approximate distributions of episodic tremor and slip (ETS) events compare favorably to margin-parallel bands of upper-plate shortening (moderately-coupled inter-plate zones) and upper-plate stability or extension (locally decoupled inter-plate zones).

In summary, the convergence-related shallow earthquakes (<30 km depth) in the upper plate of the Cascadia convergent zone are concentrated in western Washington, northwest Oregon, and southernmost British Columbia (**Figure 6(b)**). The upper-plate seismicity in Washington extends in relatively-high abundance across the Coast Ranges, Forearc valley, Cascade Range, and east of the Cascade Range to approximately 500 km landward of the buried trench. In con-

trast, upper-plate convergence-related seismicity in central and southern Oregon is sparse and only extends to about 300 km distance landward from the buried trench. The pattern of decreasing upper-plate seismicity from northern Oregon to southern Oregon is similar to decreasing upper-plate strain rates (crustal shortening) from northern Oregon to southern Oregon in the central Cascadia margin (Figure 5). It is not known whether the southward gradients of decreasing convergent strain and seismicity in the central Cascadia margin are due to 1) changes in plate convergence direction, 2) relative strengths of inter-plate coupling, and/or 3) upper-plate rigidity/strength characteristics (see further discussion below). The high abundance of shallow upper-plate earthquakes in the northern part of the central Cascadia margin differs from most other subduction zone margins (*e.g.*, Alaska, Japan, Chile) where most of the earthquakes are in the inter-plate or subducting slab regions [37].

3.4.1. Episodic Tremor and Slip (ETS) Events

A total of about 400,000 ETS events (from 2009-2018) in the Cascadia convergent zone are plotted in Figure 7. Estimated hypocenter locations for all ETS events (Figure 7(a)) show a band of intermittent inter-plate coupling along the Coast Ranges and forearc valleys of the Cascadia margin. Some elastic strain release is associated with the ETS events though, components of aseismic slip might also occur in the ETS band. The ETS band, about 100 km in width, demonstrates active elastic strain accumulation (deformation) in the upper-plate at or near the inter-plate interface, by way of the episodic release of some strain. The ETS band compares well to the zone of elevated upper-plate strain (Figure 5) that is reported to occur across the Coast Ranges in the Cascadia margin [22] [24].

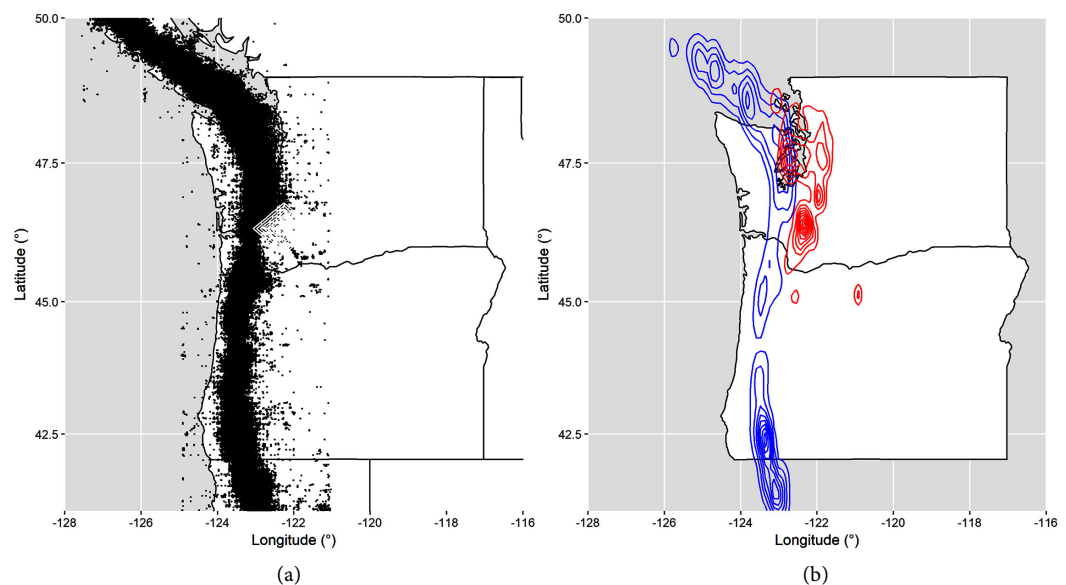


Figure 7. (a) The distribution of ETS events in the Pacific Northwest [29] [50], and (b) The density of earthquakes (red) and ETS events (blue) in the Cascadia margin.

The frequency distributions or densities of ETS events in the Cascadia margin (**Figure 7(b)**) demonstrate an important aspect of weakened inter-plate coupling on the landward (eastern) side of the Coast Range ETS band. The highest frequency of ETS events occur in the positions of forearc valleys in the central Cascadia margin, which correspond to the band of minimum convergent strain rates (**Figure 5**) and the assumed zone of inter-plate decoupling (**Figure 2**) between the Coast Ranges and the Cascade Range [22] [31]. The band of high-density ETS events narrows from north to south in the Cascadia margin, but is nearly continuous along the length of the margin. The landward side of the high-density ETS band in Washington overlaps with the zone of greatest upper-plate earthquake density in the Cascadia margin (**Figure 7(b)**). Apparently, enough upper-plate stress is propagated across the high-density ETS zone to sustain convergent seismicity landward (east) of the high-density ETS band. The same argument applies to the propagation of convergent stress in the upper-plate across the episodically decoupled zone below the forearc valleys (**Figure 2**).

3.4.2. GPS Vertical Velocities

GPS station vertical velocities for the northern and southern Cascadia convergence zone region are shown in **Figure 8**. Bands of regional uplift and subsidence, relative to the mean, occur, respectively, in the Coast Ranges and the Cascade volcanic arc. However, the regional bands of uplift and subsidence are discontinuous and irregular in outline. For example, the band of subsidence widens to encompass several basins and troughs in the central and eastern portions of Washington. The band of vertical deformation along the coast does not consistently reflect the vertical displacements that would be expected from inter-seismic strain accumulating in the mega-fold. For example, a center of high coastal uplift is shown at the Oregon and California border, located near the predicted 1st zero-isobase. A center of subsidence is shown in southwest Washington, located in the vicinity of the expected ridge of inter-seismic uplift (**Figure 2**). These contrary relations are interpreted to represent a late-stage of inter-seismic strain accumulation that persists after the initial deformation (~100 - 200 years) of the mega-fold development, following the last Cascadia mega-thrust rupture in AD 1700. However, the generally north-south trending bands of uplift (Coast Ranges) and subsidence (Cascade Range—discounting some volcano hot-spots) are interpreted to reflect convergence stress/strain relations across the Cascadia convergent zone [24].

3.4.3. Selected Across-Margin Profiles (Cross-Sections) of Integrated Datasets

In this section, the different datasets demonstrating convergent stress/strain in the central Cascadia margin are integrated by way of selected east-west profiles or cross-sections through the convergent zone. These integrated relations are used to confirm a primary (mega-scale) seismogenic structure model for Cascadia convergence zone. The implications for such a primary seismogenic structure are

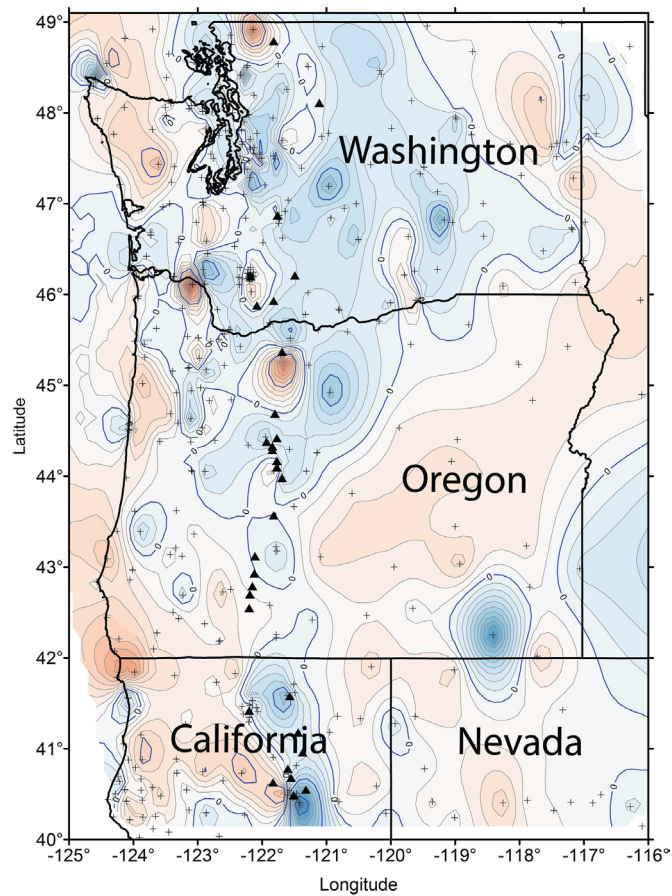


Figure 8. Map of GPS vertical velocity sites (solid dots) and velocity contours (colors) are shown for the central and southern Cascadia margin regions. The vertical velocities are contoured at $1 \text{ mm}\cdot\text{yr}^{-1}$ interval, relative to the study area mean, as defined as zero velocity for this article. Positive vertical velocity (upwards) and negative vertical velocity (downwards), respectively are shown by warm and cool colors. Figure after Cruikshank and Peterson [24].

considered in terms of seismic hazard to inland metropolitan centers and are compared to other interpretations of great earthquake seismic energy sources in the Cascadia margin. The east-west profiles of the integrated datasets were created for four latitudes between 47°N and 48°N , which contains the region of greatest changes in convergent strain and convergent seismicity from North to South (**Figures 9-12**).

The specific latitudes chosen were 47.5°N (Seattle Line), 46.5°N (Long Beach Line), 45.5°N (Portland Line), and 43.0°N (Crater Lake Line). The northern-most three plots use data within 0.5° of the center latitudes (approx. 55 km on either side). The fourth line (Crater Lake) consists of all data within 1° of 43.0°N . These four profiles show the variation in the cross-margin strain, vertical velocities, and earthquakes from north to south (**Figures 9-12**).

The upper-plate convergence strains are shown as a shortening (negative) in the Coast Ranges and locally in the Cascade Range in the Seattle (**Figure 9**) and Long Beach (**Figure 10**) profiles, where earthquake hypocenters in the upper-

and lower-plates approach the apparent inter-plate interface. Upper-plate convergent strains generally diminish on the landward (east) side of the Cascade Range where the descending slab decouples from the upper-plate, as demonstrated by deepening lower-plate earthquake hypocenters in **Figure 9**. The likely detachment of the lower-plate is not well resolved in the vicinities of the Cascade Range in the remaining profiles (**Figures 10-12**) due to a paucity of deep earthquakes there. However, small clusters of shallow earthquakes do occur at locations well landward of the volcanic arc in the three northern profiles (**Figures 9-11**). These small isolated clusters could signify minor amounts of convergent stress/strain that accumulated in localized upper-plate structures (thrusts) located well landward of the volcanic arc, some 400 km from the buried trench.

3.5. Discussion

3.5.1. Across-Margin Variations in the Cascadia Primary Seismogenic Structure

The across-margin variations in the Cascadia convergent zone that are addressed in this article are largely based on observations from 1) the upper-plate, including

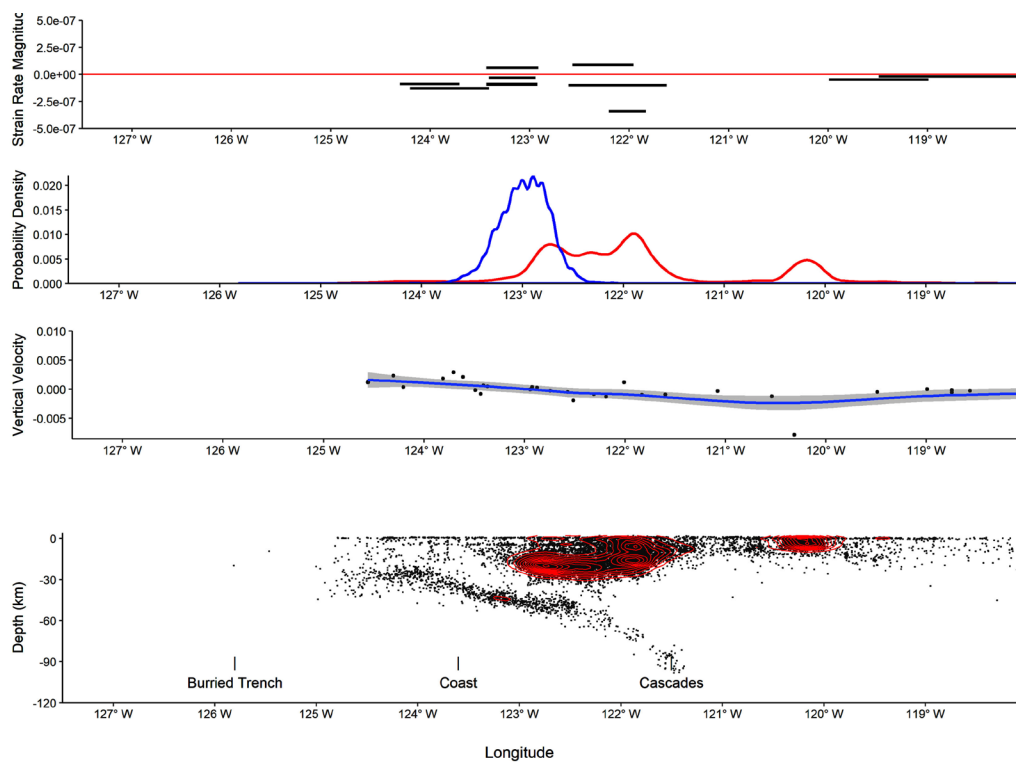


Figure 9. The Seattle transect. Data plots include 1) extents of upper-plate surface strains (east-west) reflecting crustal shortening (negative strain) and crustal lengthening (positive strain) in the upper panel, 2) frequencies (probability) of deeper earthquakes (>30 km depth) as represented by the blue line and shallow earthquakes (<30 km depth) from the upper-plate as represented by the red line in the upper-middle panel, 3) GPS vertical velocities relative to the mean with GPS station locations in the lower-middle panel, and 4) earthquake hypocenter locations and depths, contoured (red) for relative density in the lower panel. Across-margin positions are shown relative to the buried trench, coastline and Cascade volcanic arc.

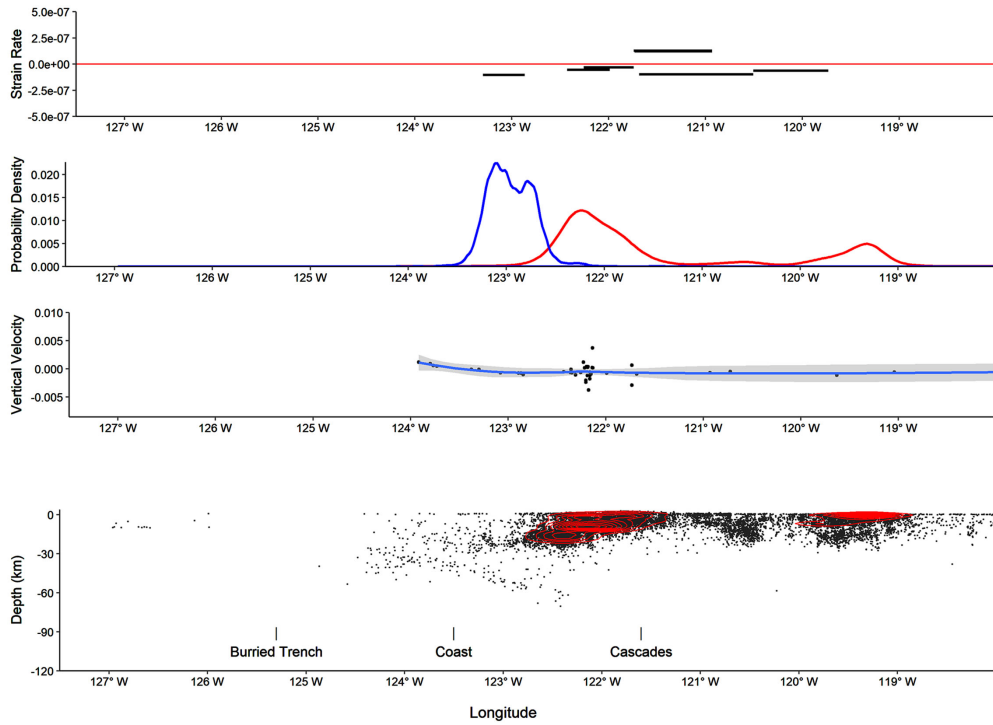


Figure 10. Long Beach line. The various plots are described in the caption for **Figure 9**. The epicenter profile shows there is a significant west dipping boundary that would be near the surface east of the Cascades, and in the region where the West-East horizontal strain increases.

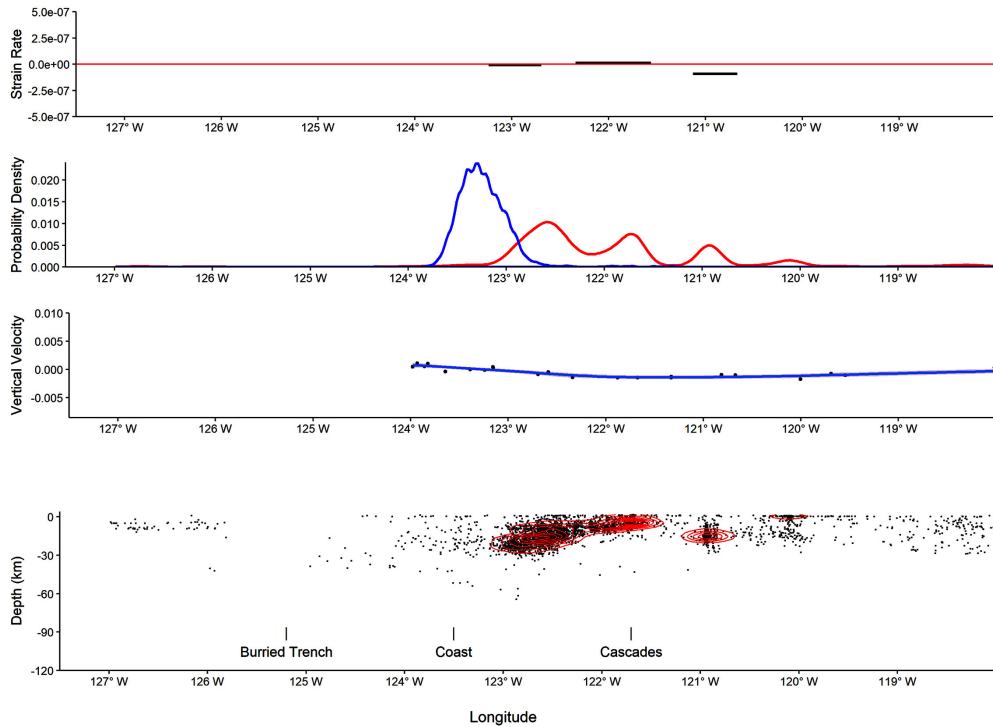


Figure 11. Portland line. The various plots are described in the caption for **Figure 9**. The epicenter profile shows there is a significant west dipping boundary that would be near the surface east of the Cascades, and in the region where the West-East horizontal strain increases. Along this profile, this westward dipping structure is more apparent than the Wadati-Benioff zone.

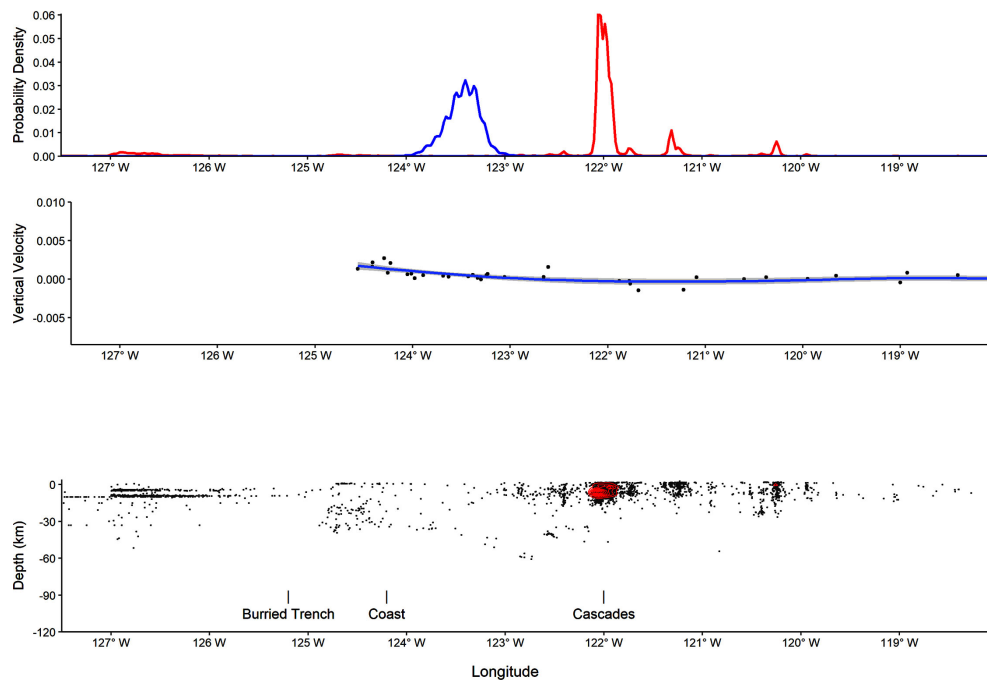


Figure 12. Crater Lake line. The various plots are described in the caption for **Figure 9**. The ETS band is still present, although in this area the Wadati-Benioff zone is less distinct than in the other profiles.

strain and seismicity, and 2) the inter-plate zone, as inferred from upper-plate deformation and ETS events. However, it can be viewed that the deformations observed in the upper-plate are the result of its being worked on by frictional coupling and differential shearing with the lower plate. The reciprocal deformations that must be occurring in the descending, or over-ridden, lower-plate are of importance to intra-slab seismicity in the lower-plate, but they are not addressed in this article.

The Coast Ranges and possibly the offshore inter-plate coupled zones (**Figure 2**) could be considered under some criteria to be “weakly coupled” due to 1) widespread occurrence of ETS events, 2) a general lack of inter-plate earthquakes, and 3) likely, some aseismic slip [24]. However, the very-low angles of subduction ($\leq 12^\circ$) yield an extraordinary-wide zone of inter-plate coupling (**Figure 2**, **Figures 9-11**). The time and distance-averaged shear-stresses generated by such great widths of inter-plate coupling could overcome the transient slip events in the coupled zone to yield the high convergent strain rates observed across the Coast Range areas (**Figure 5**). Due to the great widths of seaward inter-plate coupling, extending about 200 km landward of the trench (**Figure 7(a)**), we do not refer to the western side of the Cascadia primary seismicogenic structure as “weakly-coupled,” but rather as variably-coupled or just coupled. We do not identify or introduce the need for “completely locked-zones” within the broader coupled zones of the Cascadia primary seismicogenic structure. Much of the great earthquake energy derives from the release of the broadly distributed accumulated strain in the upper-plate, as shown for the 2011 Tohoku earth-

quake, Japan [26] and, more generally, in **Figure 4** of this article. Therefore, some previously reported estimates of inland shaking strength in the Cascadia margin, as based on seismic energy attenuation from an “assumed” narrow offshore “locked zone” [65], might be inaccurate. That is to say that the strength of shaking could be greater in the inland forearc valleys of the Cascadia convergence zone than previously thought, thus conforming to the large paleo-liquefaction/fluidization features found there [25].

A nearly-continuous band of concentrated ETS events under the forearc valleys of the Cascadia convergence zone (**Figure 7(b)**) is interpreted to represent a zone of partial inter-plate decoupling. Some of the lowest convergence strain rates on the western side of the Cascadia convergence zone (**Figure 5**) are found there [22] [24]. The occurrence of ETS events requires that some inter-plate coupling is required to achieve the accumulated elastic strain that is then released by the ETS events. Even in the zone of concentrated ETS events, under the forearc valleys, some inter-plate coupling occurs. As will be addressed further below, some inter-plate recoupling is interpreted to occur under the Cascade volcanic arc in Washington and northernmost Oregon, on the bases of 1) locally increased convergence strain rates, 2) lower concentrations of ETS events, and 3) increased seismicity in the upper-plate, which extends beyond the active volcanic areas (**Figures 5-7**). In Washington, some of these phenomena extend landward (east) of the current volcanic arc, suggesting some stress/strain propagation into the retro-arc region through the upper plate. Localized concentrations of upper-plate seismicity in the retro-arc areas (**Figures 9-11**) could indicate stress risers at “back-stop” structures, though more work is needed to establish the nature of such features. These relations raise an important question about the landward continuity of elastic strain release from mega-thrust ruptures in Washington and northernmost Oregon. Does elastic strain release from great earthquakes extend across the zone of inter-plate re-coupling under the Cascade Range in Washington and northernmost Oregon, thus significantly widening great earthquake seismic source areas in the northern half of the central Cascadia margin?

3.6. Along-Margin Variations in the Central Cascadia Primary Seismogenic Structure

Two striking features of the Cascadia primary seismogenic structure in the central margin (Juan De Fuca Plate segment) area are 1) the relatively constant widths of the uplifted Coast Ranges (**Figure 1**) and the corresponding broad band of ETS events (**Figure 1** and **Figure 7(a)**) and 2) the substantial differences in earthquake frequency between Washington/northern Oregon and central/southern Oregon (**Figure 6** and **Figure 7(b)**). Some of the upper- and lower-plate seismicity in Northwest Washington could result from the sharp bend (nearly 45°) of the plate margin in that area (**Figure 1**) and the associated confining forces associated with subduction and inter-plate coupling there. Whereas the Olympic Coast Range reaches greater elevations than the more southward

Coast Ranges in Washington and Oregon [25] the approximate widths of the uplifted ranges remain relatively similar (~100 km) along the length of the central margin. The band of ETS events only slightly widens in northern Washington and southern Oregon, relative to central Oregon, suggesting similar widths of inter-plate coupling seaward (west) of the forearc valleys (**Figure 7(a)**). So what could give rise to the abundance of upper-plate and inter-plate earthquakes in the forearc valley, Cascade Range, and especially the retro-arc areas Washington and northernmost Oregon relative to the southern half of the central and southern Oregon (**Figure 6** and **Figure 7(b)**)? The answer could be indicated by the changing convergence strain rates in the Cascade Range: locally high-rates in the North Cascades (north of the Columbia River) and generally-low rates in the South Cascades (south of the Columbia River) (**Figure 1** and **Figure 5**). The inter-plate recoupling is apparently greater under the North Cascade Range than the South Cascade Range, thereby yielding more convergence strain and seismicity in Washington and northernmost Oregon, relative to central and southern Oregon. Do the apparent differences in inter-plate recoupling signify greater upper-plate thickness/rigidity under the North Cascades than the South Cascades? Is it only a coincidence that the retro-arc Columbia River in Washington cuts across (is antecedent) through the volcanic arc at about the same position as the change in upper-plate seismicity and modern strain rates? Or are all three conditions related to changes in upper-plate thickness and inter-plate recoupling at about the latitude of Portland, Oregon?

Less-striking along-margin variations in the Cascadia primary seismogenic structure include the relative densities of ETS events at the landward (eastern) side of the ETS band (**Figure 7(b)**). Slightly higher-densities are shown in northern Washington and southern Oregon/northern California, relative to central Oregon. The higher-density ETS contours that are presented in this article are not short ellipses, as suggested by Bodmer, Toomey [66], but rather are substantially elongated along-margin. Bodmer, Toomey [66] propose that the concentrated ETS clusters are associated with relatively greater inter-plate coupling, but modern convergence strain rates in the upper-plate (**Figure 5**) do not support that hypothesis. The greatest density of ETS events occurs in the southern Cascadia margin, the Gorda Plate segment, where upper-plate convergence strain rates are moderate by comparison to the central Cascadia margin [24]. Bodmer, Toomey [66] also suggest that the northern high-density clusters of ETS events could represent along-margin segmentation of the inter-plate coupled zone, thus limiting mega-thrust rupture lengths. The rupture boundary proposed by Bodmer, Toomey [66] is between the southern end of the Olympic Range and the Northern Coast Range in southwest Washington and Oregon (**Figure 1**). Ironically, the best paleo-seismic records of along-margin ruptures occur across that proposed boundary, with at least 5 out of the last 6 major mega-thrust ruptures, during the last ~2.6 ka, crossing from the central Washington coast to the northern Oregon coast [23] [61] [63], and 3 out of the last 4 major mega-thrust ruptures, during the last 1.3 ka, crossing from the northern

Washington coast to the central Oregon coast [67]. The apparent along-margin clustering of ETS events at the eastern margin of the ETS band does not apparently reflect either 1) the strength of inter-plate coupling or 2) major mega-thrust rupture lengths from the coupled zone located seaward (west) of the forearc valleys in the central Cascadia margin.

3.7. Catastrophic Elastic Strain Release in the Cascadia Primary Seismogenic Structure

Comparing modern Cascadia upper-plate strains to those reported for the 2011 Tōhoku, Japan great earthquake ($M_w \sim 9$) we would expect only about 100 years of present convergent strain rates in the central Cascadia margin to build up to $M_w \sim 9$ energy-equivalent levels [24]. If we consider ~ 450 years to be the mean recurrence interval of major mega-thrust ruptures ($M_w 9$) and associated margin-long paleotsunami inundations in the Cascadia convergence zone [60] [68], then less than 50 years could be sufficient to accumulate sufficient elastic strain to produce a lower-magnitude ($M 8.0$) event, at the observed strain rates. However, no great earthquakes ($M_w \geq 8.0$) have occurred during the 300 years since the last major mega-thrust rupture at AD 1700 [68]. Some smaller-magnitude earthquakes ($M \leq 6$) have occurred in or near the coupled-plate interface of the central Cascadia margin (Figure 5, Figures 9-11) and ETS events are mapped throughout most of the interpreted coupled zone (Figure 7(a)), though maximum frequency distributions are localized (Figure 7(b)). Such “seismic” events serve to release stress and accumulated strain in the convergent zone. Most recently, changes in observed strain rates have been reported for the central Cascadia margin [24], suggesting aseismic propagation of strain across the western portion of the convergent zone. Presumably, some aseismic slip is occurring throughout the coupled plate interface, but enough shear stress is transmitted into the upper-plate to account for the modern strain accumulations monitored there. Furthermore, there has been relatively little reversal of vertical deformation associated with the mega-fold formed between the 1st and 2nd zero-isobases near the coast (Figure 2), as developed early in the present interseismic interval [24]. The complex relations noted above raise a very important issue. Such apparent historic and modern strain release processes, both seismic and aseismic, have not triggered a major mega-thrust rupture or great earthquake in the Cascadia margin, since the last great earthquake AD 1700. Such mega-thrust ruptures (hundreds of kilometers in length) are known to occur several century recurrence intervals throughout the Cascadia margin [60] [61] [62] [69] [70]. What then are the mechanisms that lead to a coseismic release of the accumulated elastic strain during the major mega-thrust ruptures? More generally, what triggers the major mega-thrust ruptures? The answer(s) to this question might be complex, involving both net accumulated strain and coincidences of multiple transient strain events. At the present time, the specific mechanisms that lead to major mega-thrust ruptures in the Cascadia primary seismogenic structure are not known.

We attribute the margin-parallel orientations of the large linear structural elements in the central Cascadia margin (**Figure 1** and **Figure 2**) to across-margin gradients of upper-plate thickness and associated plate strength. Maximum upper-plate thickness under the Cascade volcanic arc [30], sufficiently deflects the underlying Juan de Fuca oceanic plate to a depth of initial melting that feeds the arc volcanism, thereby further loading and thickening the upper-plate along the north-south volcanic arc. Slight thinning of the upper plate to the west (seaward) of the volcanic arc likely weakens inter-plate coupling along the forearc valleys, including the Puget Trough and Willamette Valley, both aligned north-south [31]. Further west (seaward) the shallowing dip angle ($7^\circ - 10^\circ$) of the subducting Juan de Fuca plate strengthens the inter-plate coupling, resulting in low-angle thrusting and/or underplating that has uplifted the Coast Range, generally striking north-south [23] [25]. Continued thinning and associated weakening of the upper plate to the west (seaward) towards the continental shelf, has permitted thrust faults and associated folds to extend to the upper-plate surface. The terminal thinning of the upper-plate occurs at the trench where pull-down, tectonic erosion, and/or burial have obscured the seaward edge of the upper plate. However, the buried trench in the central Cascadia margin is generally aligned north-south. Therefore, the north-south oriented contours of upper-plate thickness, which are inherited structural controls, have guided the 1) lower-plate melting, 2) effective inter-plate coupling, and 3) upper-plate inelastic strain to yield the north-south striking (margin parallel) topographic bands between the buried trench and the volcanic arc in the central Cascadia margin.

The unusually shallow dip angles ($5^\circ - 12^\circ$) of the subducting oceanic plate segments in the Cascadia margin (**Figure 2**) raise an interesting conundrum. Are the oceanic plate segments subducting under the over-riding North American continental plate or is the North American plate over-thrusting over the young and buoyant oceanic plate segments? Though likely important in terms of tectonic driving forces, we leave this question unanswered in this article, as the spatially variable inter-plate coupling and upper-plate strain accumulation in the Cascadia convergent zone are self-evident, regardless of the larger tectonic driving forces. As will be shown later in this article the underlying Juan De Fuca plate separates and descends below the North American plate to the east (landward) of the Cascade volcanic arc. That location of separation also demarks the landward-most possible extent of inter-plate coupling in the Cascadia convergent zone. Landward of the location of plate separation any localized convergent strain propagation further landward (east) would be transmitted entirely through the upper plate.

Substantial annual rates of convergent horizontal strain (10^{-8} a^{-1} to 10^{-7} a^{-1}) are mapped across the full widths of the Coast Ranges to the forearc valleys in the Cascadia convergent zone (**Figure 5**). Equivalent annual strain rates are assumed to extend across the continental shelf, though a lack of GPS stations located seaward of the coastline precludes direct strain measurements across the

shelf. Such high rates of annual convergent strain are also measured locally under the Cascade volcanic arc in Washington and northernmost Oregon, demonstrating effective inter-plate recoupling landward of the partially decoupled zone under the Puget and Willamette forearc valleys (Figure 2 and Figure 5). The inter-plate recoupling is interpreted to reach about 300 km distance from the buried trench in the southern Cascades of Oregon and 350 km distance from the trench in the northern Cascade terrain(s) in Washington and northernmost Oregon, as based on locally-high annual rates of convergent strain (10^{-8} a^{-1}). At greater landward distances the convergent strain rates diminish (10^{-9} a^{-1}) and are then replaced by locally high rates of west-east extension and/or north-south shortening [22] [24]. The across-margin transition from dominant west-east (convergent) shortening horizontal strain to dominant north-south shortening strain is used here to demark the landward extent of the primary seismogenic structure in the Cascadia convergent zone (Figure 13).

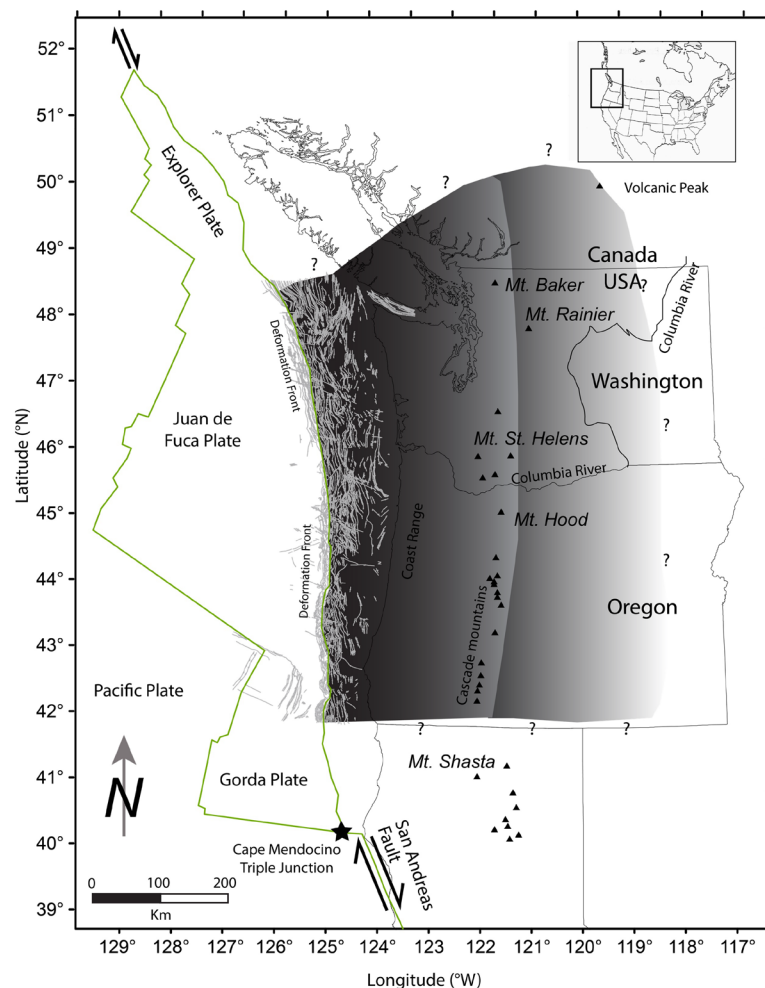


Figure 13. Approximate size and extent of the central Cascadia seismogenic structure. Strain within the structure is largest at the deformation front, and decreases east towards the Cascade mountains, then increases before decreasing again. The seismogenic structure may extend further to the east than indicated.

3.8. Regional Extent of the Central Cascadia Primary Seismogenic Structure

Horizontal strains, measured normal to plate margin orientation, represent modern convergent strain accumulation in the upper-plate of convergent margins. In this section such convergent margin strains were summarized for the central Cascadia margin, where the most complete strain data have been presented for the Cascadia subduction zone [24] and where major metropolitan centers occur in forearc valleys between the uplifting Coast Ranges and the volcanic arc (Figure 1, Figure 13). Modern annual convergent strains of 10^{-8} a^{-1} to 10^{-7} a^{-1} occur 1) regionally across the uplifting Coast Ranges to distances of 200 km from the buried trench and 2) then locally, with recoupling under the Cascades volcanic arc, to distances of up to 300 km and 450 km, respectively, in the southern and northern Cascades (Figure 5). Small, but significant, annual convergent strain rates of 10^{-9} a^{-1} occur to landward distances of nearly 500 km from the buried trench in Washington and northernmost Oregon, where the dominant strain changes from convergent (west-east) to margin parallel (north-south). For the purposes of simplification, two regional bands of modern horizontal convergent strain accumulation, including high rates and low rates, respectively are shown to extend to 300 km and 500 km in distances landward from the buried trench in the central Cascadia margin (Figure 13).

A complementary data set, to the modern horizontal strain, that demonstrates the broad extent of the Cascadia primary seismogenic structure (Figure 13) is the modern vertical deformation or GPS vertical velocities, as previously shown in Figure 8. A broadband (~100 km width) of general uplift occurs along the Olympic, North, and South Coast Ranges. A band of relative subsidence occurs landward of the Coast Ranges, but it varies substantially in across-margin width. The subsidence band is roughly centered along the Cascade volcanic arc, but it widens greatly from southern Oregon (~50 km in width) to northern Oregon (~150 km width) to Washington (~300 km width). It is not presently known whether the band of subsidence represents a continuation of across-margin mega-folding or includes a component of upper-plate pull-down by interaction with the descending plate in the inter-plate recoupled zone, located against the Cascade volcanic arc. The great width of the subsidence band in Washington is presently unexplained, but it does represent a broad region of modern elastic deformation, which coincides with the extended zone of convergent horizontal strain in Washington (Figure 5). Taken together, the along-margin bands of modern relative uplift and subsidence, and the across-margin distributions of convergent horizontal strain map out the potential extent (Figure 13) of potential seismic energy release during a major mega-thrust rupture in the Cascadia convergence zone.

4. Conclusions

A discordance between earthquake slip length/area and magnitude of energy re-

lease is shown for major inter-plate ruptures or great earthquakes in convergent margin settings worldwide. Much more energy is released from great earthquakes ($M_w > 8.0$) in convergent margins than would be expected from other neotectonic settings for equivalent rupture lengths. In convergent margin subduction zones, the elastic energy generated during interseismic inter-plate coupling is stored throughout the upper-plate, rather than just at the inter-plate interface. The coseismic release of the stored elastic strain during major megathrust ruptures accounts for the large anomalous magnitudes of earthquake energy associated with convergent margin settings in general and in subduction zones specifically. The broad area of potential coseismic energy release is defined here as a primary seismogenic structure in convergent margin settings.

The Cascadia subduction zone is shown to represent a primary seismogenic structure, with measured modern strain accumulation occurring throughout the upper-plate, to distances of several hundred kilometers landward of the buried trench. The maximum widths of horizontal strain in the central Cascadia margin coincide with the landward extent of 1) modern vertical deformation bands, 2) historic upper-plate earthquakes, and 3) broad areas of ETS events, demonstrating inter-plate coupling. Inter-plate coupling is interpreted to extend from the shelf to the forearc valleys, under the uplifting Coast Ranges. Recoupling is interpreted to occur under the landward side of the forearc valleys and across the Cascades volcanic arc, as indicated by 1) localized convergent strain, 2) a band of modern subsidence or plate pull-down, and 3) intermittent ETS events. The apparent width of the seismogenic structure increases from the southern portion of the central margin (~300 km landward of the trench) to the northern portion of the central margin (~450 km landward from the trench) based on upper-plate convergent strain. The greater width of the primary seismogenic structure in Washington and northernmost Oregon is interpreted to represent a substantially wider zone of inter-plate recoupling under the northern Cascades relative to the southern Cascades. Stronger inter-plate recoupling in western Washington relative to western Oregon could account for the increased frequency of historical earthquakes in western Washington relative to western Oregon. However, there is little north-south variation in the indices of inter-plate coupling seaward of the forearc valleys, as demonstrated by relative similarities of 1) modern strain rates, 2) widths of the uplifting Coast Ranges and 3) frequency of ETS events under the Coast Ranges in Washington and Oregon.

The great width of the coupled zones and associated accumulated elastic strain in the upper-plate of the central Cascadia margin likely account for the relatively long lengths (≥ 500 km) of most major mega-thrust ruptures, as recorded by coseismic coastal subsidence and corresponding nearfield paleotsunami inundation. Of equal concern to great earthquake magnitude is the proximity of great earthquake energy source(s), as produced across the width of the primary seismogenic structure, to inland metropolitan centers. Stronger than previously expected shaking in these metropolitan centers could occur from a future major

mega-thrust rupture due to the broad source region of coseismic energy release in the Cascadia primary seismogenic structure. Though the Cascadia margin is unusual in its low angles of inter-plate landward dip and the resulting large widths of inter-plate coupling it does demonstrate the transfer of inter-plate shear stress to elastic strain accumulation throughout the full thickness of the overlying upper-plate. In this regard, the Cascadia margin likely serves as an example of very-large or primary seismogenic structures in some other well-coupled convergent margins worldwide.

Conflicts of Interest

The authors declare no conflicts of interest regarding the publication of this paper.

References

- [1] Mason, B. (2017) New Zealand Temblor Points to Threat of Compound Quakes. *Science*, **355**, 1250-1251. <https://doi.org/10.1126/science.355.6331.1250>
- [2] Hamling, I.J., Hreinsdóttir, S., Clark, K., Elliott, J., Liang, C., Fielding, E., Litchfield, N., Villamor, P., Wallace, L., Wright, T.J., D'Anastasio, E., Bannister, S., Burbidge, D., Denys, P., Gentle, P., Howarth, J., Mueller, C., Palmer, N., Pearson, C., Power, W., Barnes, P., Barrell, D.J.A., Van Dissen, R., Langridge, R., Little, T., Nicol, A., Pettinga, J., Rowland, J. and Stirling, M. (2017) Complex Multifault Rupture during the 2016 Mw 7.8 Kaikōura Earthquake, New Zealand. *Science*, **356**, eaam7194. <https://doi.org/10.1126/science.aam7194>
- [3] Johnson, A.M., Cruikshank, K.M. and Fleming, R.W. (1994) Borrego Mountain, Loma Prieta, Landers, Northridge: Simple Earthquakes or Seismostructural Events? *EOS*, **75**, 343.
- [4] Rymer, M.J. and Ellsworth, W.L. (1990) The Coalinga, California, Earthquake of May 2, 1983. United States Geological Survey, Washington DC, 417. <https://doi.org/10.3133/pp1487>
- [5] Mavko, G.M., Schulz, S. and Brown, B.D. (1985) Effects of the 1983 Coalinga, California, Earthquake on Creep along the San Andreas Fault. *Bulletin of the Seismological Society of America*, **75**, 475-489.
- [6] Hill, M.L. (1984) Earthquakes and Folding, Coalinga, California. *Geology*, **12**, 711-712. [https://doi.org/10.1130/0091-7613\(1984\)12<711:EAFCC>2.0.CO;2](https://doi.org/10.1130/0091-7613(1984)12<711:EAFCC>2.0.CO;2)
- [7] U.S. Geological Survey (1982) The Imperial Valley, California, Earthquake of October 15, 1979. United States Geological Survey, Washington DC, 451.
- [8] Allen, C.R., Wyss, M., Brune, J.N., Grantz, A. and Wallace, R. (1972) Displacements on the Imperial, Superstition Hills, and San Andreas Faults Triggered by the Borrego Mountain Earthquake. In: Sharp, R.V., Ed., *The Borrego Mountain Earthquake of April 9, 1968*, Geological Survey Professional Paper No. 787, United States Geological Survey, Washington DC, 87-104.
- [9] Fleming, R.W. and Johnson, A.M. (1997) Growth of a Tectonic Ridge during the Landers Earthquake. *Geology*, **25**, 323-326. [https://doi.org/10.1130/0091-7613\(1997\)025<0323:GOATRD>2.3.CO;2](https://doi.org/10.1130/0091-7613(1997)025<0323:GOATRD>2.3.CO;2)
- [10] Fleming, R.W., Messerich, J.A. and Cruikshank, K.M. (1998) Fractures along a Portion of the Emerson Fault Zone Related to the 1992 Landers, California, Earthquake: Evidence for the Galway Lake Road Rotated Block. Geological Society of

America Map and Chart Series MCH082.

- [11] Johnson, A.M., Fleming, R.W., Cruikshank, K.M., Martosudarmo, S.Y., Johnson, N.A., Johnson, K.M. and Wei, W. (1997) Analecta of Structures Formed during the 28 June 1992 Landers-Big Bear, California, Earthquake Sequence. United States Geological Survey, Washington DC, 59. <https://doi.org/10.3133/ofr9794>
- [12] Julian, B.R., Miller, A.D. and Foulger, G.R. (1998) Non-Double-Couple Earthquakes. 1. Theory. *Reviews of Geophysics*, **36**, 525-549. <https://doi.org/10.1029/98RG00716>
- [13] Miller, A.D., Foulger, G.R. and Julian, B.R. (1998) Non-Double-Couple Earthquakes. 2. Observations. *Reviews of Geophysics*, **36**, 551-568. <https://doi.org/10.1029/98RG00717>
- [14] Reches, Z.E. (1978) Analysis of Faulting in Three-Dimensional Strain Field. *Tectonophysics*, **47**, 109-129. [https://doi.org/10.1016/0040-1951\(78\)90154-3](https://doi.org/10.1016/0040-1951(78)90154-3)
- [15] Healy, D., Blenkinsop, T.G., Timms, N.E., Meredith, P.G., Mitchell, T.M. and Cooke, M.L. (2015) Polymodal Faulting: Time for a New Angle on Shear Failure. *Journal of Structural Geology*, **80**, 57-71. <https://doi.org/10.1016/j.jsg.2015.08.013>
- [16] Plafker, G. (1969) Tectonics of the March 27, 1964 Alaska Earthquake. U.S. Geological Survey Professional Paper 543-I, 74 p.
- [17] Savage, J.C. (1980) Dislocations in Seismology. North-Holland Publishing Co., Amsterdam, 253-339.
- [18] Savage, J.C. (1983) A Dislocation Model of Strain Accumulation and Release at a Subduction Zone. *Journal of Geophysical Research*, **88**, 4984-4996. <https://doi.org/10.1029/JB088iB06p04984>
- [19] Vita-Finzi, C. and Mann, C.D. (1994) Seismic Folding in Coastal South Central Chile. *Journal of Geophysical Research*, **99**, 12289-12299. <https://doi.org/10.1029/93JB03061>
- [20] Plafker, G. (1972) Alaskan Earthquake of 1964 and Chilean Earthquake of 1960: Implications for Arc Tectonics. *Journal of Geophysical Research*, **77**, 901-925. <https://doi.org/10.1029/JB077i005p00901>
- [21] Wang, K., Wells, R., Mazzotti, S., Hyndman, R.D. and Sagiya, T. (2003) A Revised Dislocation Model of Interseismic Deformation of the Cascadia Subduction Zone. *Journal of Geophysical Research*, **108**, 2016-2029. <https://doi.org/10.1029/2001JB001227>
- [22] Cruikshank, K.M. and Peterson, C.D. (2015) Current State of Strain in the Central Cascadia Margin Derived from Changes in Distance between GPS Stations. *Open Journal of Earthquake Research*, **4**, 23-36. <https://doi.org/10.4236/ojer.2015.41003>
- [23] Peterson, C.D., Cruikshank, K.M. and Darienzo, M. (2012) Coastal Tectonic Strain and Paeloseismicity in the South Central Cascadia Margin, Oregon, USA. In: Vidovic, M., Ed., *Earthquakes: Triggers, Environmental Impact and Potential Hazards*, NOVA Open Access Publisher, Hauppauge, NY, 1-37.
- [24] Cruikshank, K.M. and Peterson, C.D. (2017) Late Stage Interseismic Strain Interval, Cascadia Subduction Zone Margin, USA and Canada. *Online Journal of Earthquake Research*, **6**, 1-34. <https://doi.org/10.4236/ojer.2017.61001>
- [25] Peterson, C.D., Kristensen, K. and Minor, R. (2014) Large-Scale Fluidization Features from Late Holocene Coseismic Paleoliquefaction in the Willamette River Forearc Valley, Central Cascadia Subduction Zone, Oregon, USA. *Open Journal of Earthquake Research*, **3**, 82-99. <https://doi.org/10.4236/ojer.2014.32009>
- [26] Cruikshank, K.M. and Peterson, C.D. (2013) Strain Energy Release from the 2011

- 9.0 Mw Tōhoku Earthquake, Japan. *Open Journal of Earthquake Research*, **2**, 75-83. <https://doi.org/10.4236/ojer.2013.24008>
- [27] Dragovich, J. and Harris, J. (2010) The 2010 Chile Earthquake: Observations and Research Implications. https://nehrp.gov/pdf/ppt_chile2010.pdf
- [28] Dragert, H., Hyndman, R.D., Rogers, G.C. and Wang, K. (1994) Current Deformation and the Width of the Seismogenic Zone of the Northern Cascadia Subduction Thrust. *Journal of Geophysical Research*, **99**, 653-668. <https://doi.org/10.1029/93JB02516>
- [29] Wech, A.G. (2010) Interactive Tremor Monitoring. *Seismological Research Letters*, **81**, 664-669. <https://doi.org/10.1785/gssrl.81.4.664>
- [30] Parsons, T., Blakely, R.J., Brocher, T.M., Christensen, N.I., Fisher, M.A., Flueh, E., Kilbride, F., Luetgert, J.H., Miller, K., ten Brink, U.S., Trehu, A.M. and Wells, R.E. (2005) Crustal Structure of the Cascadia Fore Arc of Washington. In: Kayen, R., Ed., *Earthquake Hazards of the Pacific Northwest Coastal and Marine Regions*, United States Geological Survey, Reston, 40. <https://doi.org/10.3133/pp1661D>
- [31] Peterson, C.D. and Cruikshank, K.M. (2014) Quaternary Tectonic Deformation, Holocene Paleoseismicity, and Modern Strain in the Unusually-Wide Coupled Zone of the Central Cascadia Margin, Washington and Oregon, USA and British Columbia, Canada. *Journal of Geography and Geology*, **6**, 33. <https://doi.org/10.5539/jgg.v6n3p1>
- [32] Goldfinger, C., Grijalva, K., Bürgmann, R., Morey, A.E., Johnson, J.E., Nelson, C.H., Gutiérrez-Pastor, J., Ericsson, A., Karabanov, E., Chaytor, J.D., Patton, J. and Gràcia, E. (2008) Late Holocene Rupture of the Northern San Andreas Fault and Possible Stress Linkage to the Cascadia Subduction Zone. *Bulletin of the Seismological Society of America*, **98**, 861-889. <https://doi.org/10.1785/0120060411>
- [33] Goldfinger, C., Nelson, C.H. and Johnson, J.E. (2003) Holocene Earthquake Records from the Cascadia Subduction Zone and Northern San Andreas Fault Based on Precise Dating of Offshore Turbidites. *Annual Review of Earth and Planetary Sciences*, **31**, 555-577. <https://doi.org/10.1146/annurev.earth.31.100901.141246>
- [34] Gomberg, J., Bedrosian, P., Bodin, P., Bostock, M., Brudzinski, M., Creager, K., Dragert, H., Egbert, G., Ghosh, A., Henton, J., Houston, H., Kao, H., McCrory, P., Melbourne, T., Peacock, S., Roeloffs, E., Rubinstein, J., Schmidt, D., Trèhu, A., Vidale, J., Wang, K. and Wech, A. (2010) Slow-Slip Phenomena in Cascadia from 2007 and Beyond: A Review. *Geological Society of America Bulletin*, **122**, 963-978. <https://doi.org/10.1130/B30287.1>
- [35] Hyndman, R.D. and Wang, K. (1995) The Rupture Zone of the Cascadia Great Earthquakes from Current Deformation and Thermal Regime. *Journal of Geophysical Research*, **100**, 22133-22154. <https://doi.org/10.1029/95JB01970>
- [36] USGS (2019) U.S. Geological Survey Earthquake Hazards Program. <https://earthquake.usgs.gov>
- [37] IRIS (2019) Incorporated Research Institutions for Seismology. <https://www.iris.edu>
- [38] CMT (2019) Global Centroid Moment Tensor Project. <https://www.globalcmt.org>
- [39] Wells, D.L. and Coppersmith, K.J. (1994) New Empirical Relationships among Magnitude, Rupture Length, Rupture Width, Rupture Area, and Surface Displacement. *Bulletin of the Seismological Society of America*, **84**, 974-1002.
- [40] Biasi, G.P., Weldon, I., Ray J. and Dawson, T.E. (2013) Distribution of Slip in Ruptures, in Uniform California Earthquake Rupture Forecast, Version 3 (UCERF3)—The Time-Independent Model. U.S. Geological Survey, Washington DC, 97. <http://pubs.usgs.gov/of/2013/1165>

- [41] Wesnousky, S.G. (2008) Displacement and Geometrical Characteristics of Earthquake Surface Ruptures: Issues and Implications for Seismic-Hazard Analysis and the Process of Earthquake Rupture. *Bulletin of the Seismological Society of America*, **98**, 1609-1632. <https://doi.org/10.1785/0120070111>
- [42] Kanamori, H. and Anderson, D.L. (1975) Theoretical Basis of Some Empirical Relations in Seismology. *Bulletin of the Seismological Society of America*, **65**, 1073-1095.
- [43] Stirling, M., Rhoades, D. and Berryman, K. (2002) Comparison of Earthquake Scaling Relations Derived from Data of the Instrumental and Preinstrumental Era. *Bulletin of the Seismological Society of America*, **92**, 812-830. <https://doi.org/10.1785/0120000221>
- [44] Young, J.B., Presgrave, B.W., Aichele, H., Wiens, D.A. and Flinn, E.A. (1996) The Flinn-Engdahl Regionalisation Scheme: The 1995 Revision. *Physics of the Earth and Planetary Interiors*, **96**, 223-297. [https://doi.org/10.1016/0031-9201\(96\)03141-X](https://doi.org/10.1016/0031-9201(96)03141-X)
- [45] Frohlich, C. (2006) Deep Earthquakes. Cambridge University Press, Cambridge. <https://doi.org/10.1017/CBO9781107297562>
- [46] PNSN (2019) Pacific Northwest Seismic Network. <https://pnsn.org>
- [47] Kagan, Y.Y. (1997) Seismic Moment-Frequency Relation for Shallow Earthquakes: Regional Comparison. *Journal of Geophysical Research*, **102**, 2835-2852. <https://doi.org/10.1029/96JB03386>
- [48] SPUD (2019) The Searchable Product Depository. <http://ds.iris.edu/spud>
- [49] Choy, G.L. and Boatwright, J.L. (2002) Radiated Seismic Energy and Energy Magnitude, in U.S. Geological Survey Information Sheet. U.S. Geological Survey, Denver.
- [50] Wech, A.G. and Creager, K.C. (2008) Automated Detection and Location of Cascadia Tremor. *Geophysical Research Letters*, **35**, L20302. <https://doi.org/10.1029/2008GL035458>
- [51] Rogers, G. and Dragert, H. (2003) Episodic Tremor and Slip on the Cascadia Subduction Zone: The Chatter of Silent Slip. *Science*, **300**, 1942-1943. <https://doi.org/10.1126/science.1084783>
- [52] UNAVCO (2016) University Navstar Consortium. <http://www.unavco.org>
- [53] Burgette, R.J., Weldon II, R.J. and Schmidt, D.A. (2009) Interseismic Uplift Rates for Western Oregon and Along-Strike Variation in Locking on the Cascadia Subduction Zone. *Journal of Geophysical Research*, **114**, 24. <https://doi.org/10.1029/2008JB005679>
- [54] Shaw, B.E. (2013) Earthquake Surface Slip-Length Data Is Fit by Constant Stress Drop and Is Useful for Seismic Hazard Analysis. *Bulletin of the Seismological Society of America*, **103**, 876-893. <https://doi.org/10.1785/0120110258>
- [55] Cowie, P.A. and Scholtz, C.H. (1992) Displacement-Length Scaling Relationship for Faults: Data Synthesis and Discussion. *Journal of Structural Geology*, **14**, 1149-1156. [https://doi.org/10.1016/0191-8141\(92\)90066-6](https://doi.org/10.1016/0191-8141(92)90066-6)
- [56] Tufte, E.R. (2001) The Visual Display of Quantitative Information. Second Edition, Graphics Press, Cheshire, 200.
- [57] Matta, C.F., Massa, L., Gubskaya, A.V. and Knoll, E. (2011) Can One Take the Logarithm or the Sine of a Dimensioned Quantity or a Unit? Dimensional Analysis Involving Transcendental Functions. *Journal of Chemical Education*, **88**, 67-70. <https://doi.org/10.1021/ed1000476>
- [58] Stein, S. and Wysession, M. (2003) An Introduction to Seismology, Earthquakes,

and Earth Structure. Blackwell, Malden, 498.

- [59] Peterson, C.D., Darienzo, M.E., Doyle, D.L. and Barnett, E.T. (1995) Evidence for Coseismic Subsidence and Tsunamis Inundation during the Past 3000 Years at Siletz Bay, Oregon. In: Priest, G.R., Ed., *Explanation of Mapping Methods and Use of the Tsunami Hazard Map of the Siletz Bay Area, Lincoln County, Oregon*, Oregon Department of Geology and Mineral Industries, Portland, 45-69.
- [60] Peterson, C.D., Clague, J.J., Carver, G.A. and Cruikshank, K.M. (2013) Recurrence Intervals of Major Paleotsunamis as Calibrated by Historic Tsunami Deposits in Three Localities: Port Alberni, Cannon Beach, and Crescent City, along the Cascadia Margin, Canada and USA. *Natural Hazards*, **68**, 321-336.
<https://doi.org/10.1007/s11069-013-0622-1>
- [61] Atwater, B.F., Tuttle, M.P., Schweig, E.S., Rubin, C.M., Yamaguchi, D.K. and Hemphill-Halley, I. (2004) Earthquake Recurrence, Inferred from Paleoseismology. In: Gillespie, A.R., Porter, S.C. and Atwater, B.F., Eds., *The Quaternary Period in the United States*, Elsevier, Amsterdam, 331-350.
[https://doi.org/10.1016/S1571-0866\(03\)01015-7](https://doi.org/10.1016/S1571-0866(03)01015-7)
- [62] Darienzo, M.E. and Peterson, C.D. (1995) Magnitude and Frequency of Subduction-Zone Earthquakes along the Northern Oregon Coast in the Past 3,000 Years. *Oregon Geology*, **57**, 3-12.
- [63] Peterson, C.D., Carver, G.A., Clague, J.J. and Cruikshank, K.M. (2015) Maximum-Recorded Overland Run-Ups of Major Nearfield Paleotsunamis during the Past 3000 Years along the Cascadia Margin, USA, and Canada. *Natural Hazards*, **77**, 2005-2026. <https://doi.org/10.1007/s11069-015-1689-7>
- [64] Peterson, C.D. and Madin, I.P. (1997) Coseismic Paleoliquifaction Evidence in the Central Cascadia Margin. *Oregon Geology*, **59**, 51-74.
- [65] McCaffrey, R., Long, M.D., Goldfinger, C., Zwick, P.C., Nabelek, J.L., Johnson, C.K. and Smith, C. (2000) Rotation and Plate Locking at the Southern Cascadia Subduction Zone. *Geophysical Research Letters*, **27**, 3117-3120.
<https://doi.org/10.1029/2000GL011768>
- [66] Bodmer, M., Toomey, D.R., Hooft, E.E.E. and Schmandt, B. (2018) Buoyant Asthenosphere beneath Cascadia Influences Megathrust Segmentation. *Geophysical Research Letters*, **45**, 6954-6962. <https://doi.org/10.1029/2018GL078700>
- [67] Peterson, C.D., Cruikshank, K.M., Darienzo, M.E., Wessen, G., Butler, V. and Sterling, S. (2013) Coseismic Subsidence and Paleotsunami Runup Records from Latest Holocene Deposits in the Waatch Valley, Neah Bay, Northwest Washington, USA: Links to Great Earthquakes in the Northern Cascadia Margin. *Journal of Coastal Research*, **29**, 157-172. <https://doi.org/10.2112/JCOASTRES-D-12-00031.1>
- [68] Satake, K., Shimazaki, K., Tsuji, Y. and Ueda, K. (1996) Time and Size of Giant Earthquake in Cascadia Inferred from Japanese Tsunami Records of January 1700. *Nature*, **378**, 246-249. <https://doi.org/10.1038/379246a0>
- [69] Hutchinson, I. and Clague, J. (2017) Were They All Giants? Perspectives on Late Holocene Plate-Boundary Earthquakes at the Northern End of the Cascadia Subduction Zone. *Quaternary Science Reviews*, **169**, 29-49.
<https://doi.org/10.1016/j.quascirev.2017.05.015>
- [70] Adams, J. (1996) Great Earthquakes Recorded by Turbidites off the Oregon-Washington Coast. In: Rodgers, A.M., Walsh, T.J., Kockelman, W.J. and Priest, G.R., Eds., *Assessing Earthquake Hazards and Reducing Risk in the Pacific Northwest*, United States Geological Survey, Washington DC, 147-158.